eScience 6 (2026) 100589

Contents lists available at ScienceDirect

eScience

journal homepage: www.keaipublishing.com/en/journals/escience

Review

A microscopic view of diffusion and failure mechanisms of lithium anodes in solid-state batteries

Luca Weckelmann[a,b], Hao Lyu[c,*], Han Yang[a,b], Chih-Long Tsai[a,*], Krzysztof Dzieciol[a], Shicheng Yu[a], Anna Windmüller[a], Hans Kungl[a], Zhenan Bao[c], Rüdiger-A. Eichel[a,b]

[a] Institute of Energy Technologies - Fundamental Electrochemistry (IET-1), Forschungszentrum Jülich GmbH, Jülich 52428, Germany
[b] Institute of Physical Chemistry, RWTH Aachen University, Aachen 52075, Germany
[c] Department of Chemical Engineering, Stanford University, Stanford, CA 94305, USA

HIGHLIGHTS

- This review establishes correlations between key parameters and processes governing dendrite growth in solid electrolytes.
- It studies physicochemical causes of degradation, their evolution during cycling, and effects on cell performance.
- Low lithium self-diffusion, coupled with interfacial inhomogeneities, is identified as a key driver for dendrite formation.

GRAPHICAL ABSTRACT

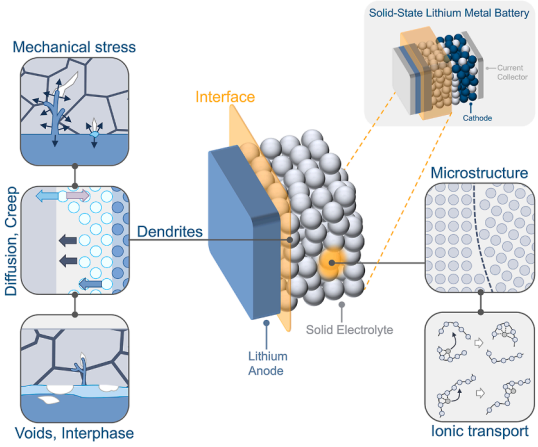

ARTICLE INFO

Keywords:
Lithium metal anode
Solid electrolyte
Dendrite
Diffusion
All-solid-state batteries

ABSTRACT

Although all-solid-state lithium metal batteries (SSLBs) have long been regarded as successors of the commercially available lithium-ion batteries (LIBs), SSLBs do not yet deliver sufficient and competitive performance. The use of a solid electrolyte in combination with lithium metal as the anode increases the theoretical energy density and improves safety. However, these advantages are overshadowed by various degradation mechanisms—especially dendrite formation. Hence, comprehending the phenomenon of dendrite nucleation and growth will be a decisive step toward the commercialization of SSLBs. This review summarizes the current understanding of dendrite formation at the solid electrolyte/lithium metal anode interface. Focusing on the microscopic level, it aims to compare and categorize different findings related to dendrite formation in inorganic, polymer (including dynamic and dynamic-crosslinked polymer), and hybrid solid electrolyte batteries. Different critical mechanisms are highlighted, such as inhomogeneous plating or stripping, as well as the interconnections

* Corresponding authors.
E-mail addresses: haolyu@stanford.edu (H. Lyu), c.tsai@fz-juelich.de (C.-L. Tsai).
Peer review under the responsibility of Editorial Board of eScience.

https://doi.org/10.1016/j.esci.2026.100589
Received 10 November 2025; Received in revised form 1 March 2026; Accepted 28 April 2026
Available online 7 May 2026

between those failure mechanisms. Processes that result in dendrite formation or are a consequence of dendrite formation are included, and key mechanisms such as ionic transport, homogeneous plating and stripping, as well as interphase evolution and its connection to failure mechanisms are reviewed.

1. Introduction

The development of better batteries in terms of higher safety, higher energy density, faster charging, and longer lifetime is one crucial step for progressive electrification. However, current commercially available lithium-ion batteries (LIBs), currently regarded as state-of-the-art, have limitations in relation to these requirements [1]. One reason is their use of liquid electrolytes [2,3], which are usually accompanied by several safety concerns, such as possible leakage of toxic liquid electrolyte, or thermal runaway caused by mechanical, thermal, or electrical abuse [4, 5]. To minimize hazards, alternative battery models must be developed. A highly promising type is the all-solid-state battery, utilizing solid materials as the electrolyte [6]. Compared to their liquid counterparts, solid-state electrolytes are less prone to hazardous events due to their intrinsic lower or non-flammability and absence of liquids [7]. When the solid electrolyte comes in contact with the lithium metal anode, a stable solid–electrolyte interface (SEI) can be formed, which contributes to a stable potential and less active material consumption during operation. In contrast, the SEI in liquid electrolytes continues to grow due to the infiltration of liquid into SEI cracks, ultimately reaching the lithium anode [8,9]. Therefore, the use of solid electrolytes potentially opens up the possibility of using lithium metal as the anode for higher-density batteries.

The advantage of using lithium metal as the anode for a lithium battery is the possible higher theoretical energy density, offering the opportunity for creating higher voltage cells and enabling faster charging [10]. Compared to commonly used graphite anodes, a lithium metal anode allows the achievement of a cell-level gravimetric energy density of 454 Wh kg^{-1}, whereas the graphite anode is limited to 314 Wh kg^{-1} when paired with a lithium nickel cobalt aluminum oxide (NCA, e.g., $LiNi_{0.8}Co_{0.15}Al_{0.05}O_2$) cathode [11]. Likewise, the volumetric cell-level energy density can be nearly doubled with lithium metal anodes (1392 Wh L^{-1}) compared to graphite anodes (773 Wh L^{-1}) with the same cell chemistry. In addition, the high reduction potential of lithium metal (−3.04 V vs. standard electrode potential) creates the opportunity for fabricating high-voltage cells in terms of theoretically possible potential differences to the known cathode materials. Moreover, a lithium metal anode can empower fast charging by using metal electroplating as the charging mechanism, instead of relying on intercalation diffusion like in the conventional anodes for LIBs [12,13].

Despite their theoretically promising properties, competitive all-solid-state lithium metal batteries (SSLBs) are not commercially available yet. One of the main reasons is the occurrence of dendrites during electrochemical cycling [14–16]. Dendrites result from undesirable lithium filament growth inside a battery cell. Cell cycling with high current densities accelerates dendrite formation, which can lead to a short circuit. For example, battery cells consisting of oxide-class solid-state electrolytes such as $Li_7La_3Zr_2O_{12}$ (LLZO), and sulfide-class solid-state electrolytes such as $Li_7P_3S_{11}$ (LPS), often fail due to dendrite formation at a current density less than 1 mA cm^{-2} and thus are not competitive with liquid electrolytes, which can operate in the range of 4–10 mA cm^{-2} at room temperature [17]. Although the lower dendrite formation current densities of SSLBs could be relative to the ionic conductivity of the electrolytes, recent developments in inorganic solid electrolytes (e.g. sulfide-class solid electrolytes 10^{-2}–10^{-4} S cm^{-1}) can keep up with the performance of liquid electrolytes with high ionic conductivities in the range of 10^{-2} S cm^{-1} [18–20]. Soft, polymer-based solid-state electrolytes represent a complementary approach to mitigate interfacial failures induced dendrites by maintaining conformable electrolyte contact; however, their conduction of lithium ions, in the absence of plasticizers, depends heavily on the polymers' segmental motion, critically limiting their ionic conductivities to a representative level of 10^{-4}–10^{-6} S cm^{-1}at room temperature [18–20]. Very low lithium self-diffusion in the lithium anode and poor solid electrolyte/electrode interfaces without any free-moving liquid phase are acknowledged as the main reasons for a restricted low operational current density and cycling performance. Although the problem of dendrites has been known for a long time, the nucleation and propagation mechanisms are still not fully understood and remain subjects of current research [21].

An inevitable step for advancing SSLBs is to disentangle the dependencies of critical parameters and processes that lead to dendrite formation when the solid electrolyte, the lithium anode, and their interface are involved. To offer a complete survey, we consider all types of solid electrolytes: inorganic, polymer—including dynamic and dynamic-crosslinked polymers—and hybrid solid electrolytes. This review pays special attention to clarifying and connecting current understandings from the microscopic perspective.

2. Ionic transport on an atomic level

The transport mechanism of lithium ions inside a solid electrolyte can be driven by thermal energy leading to diffusion, electrical energy leading to migration, or mechanical external pressure leading to convection [22]. For inorganic solid electrolytes, which include oxides, sulfides, and halides, the underlying atomic-scale transport mechanism is ion hopping. Defects in the crystal lattice enable the diffusion mechanism; they may show up as a point, line, planar, volume, or electron defect and affect the ionic transport properties significantly [18,23]. Among these, point defects, especially vacancies and interstitial defects, play a crucial role in ionic conduction. Due to the different defect types, three main transport mechanisms are possible: vacancy, interstitial, and interstitial–substitutional exchange hopping (knock-on mechanism) (Fig. 1a) [23–25].

Without an external electric field and mechanical pressure, the only transport process for ions is diffusion. Diffusion depends on a diffusion coefficient D, which is proportional to the hopping frequency ν. The hopping frequency is strongly affected by the required energy E_h for a jump between the ionic sites at a temperature T. Since the activation energy is provided by thermal energy, the hopping frequency for a certain temperature follows the Boltzmann distribution. This leads to the use of the Arrhenius equation:

$$\nu = \nu_0 e^{-\frac{E_h}{k_B T}} \tag{1}$$

where ν_0 is the attempt frequency and k_B is the Boltzmann constant. From the Nernst–Einstein equation, the relation between ionic conductivity σ and diffusion coefficient D_σ is derived for non-interacting ionic migration to $\sigma = D_\sigma(T) n(T) q^2 / k_B T$, which states that besides the quantity of charge per ion q, the ionic conductivity is also linear, depending on the charge carrier density n [26]. At this point, it needs to be mentioned that the equation is only an approximation but in most cases is correct [27,28]. Forming a vacancy requires an activation energy E_v and can also be expressed with the foregoing Arrhenius equation (1). Combining both the activation energy for vacancy formation and the hopping of an ion leads to $E_a = E_v + E_h$, with E_a as the experimentally measured activation energy for the conduction process. This, in turn, results in the proportionality of $\sigma \sim e^{-E_a/k_B T}$, where σ is the ionic conductivity in inorganic solids for the case of direct and uncorrelated migration [29, 30]. A temperature increase not only increases the ionic conductivity

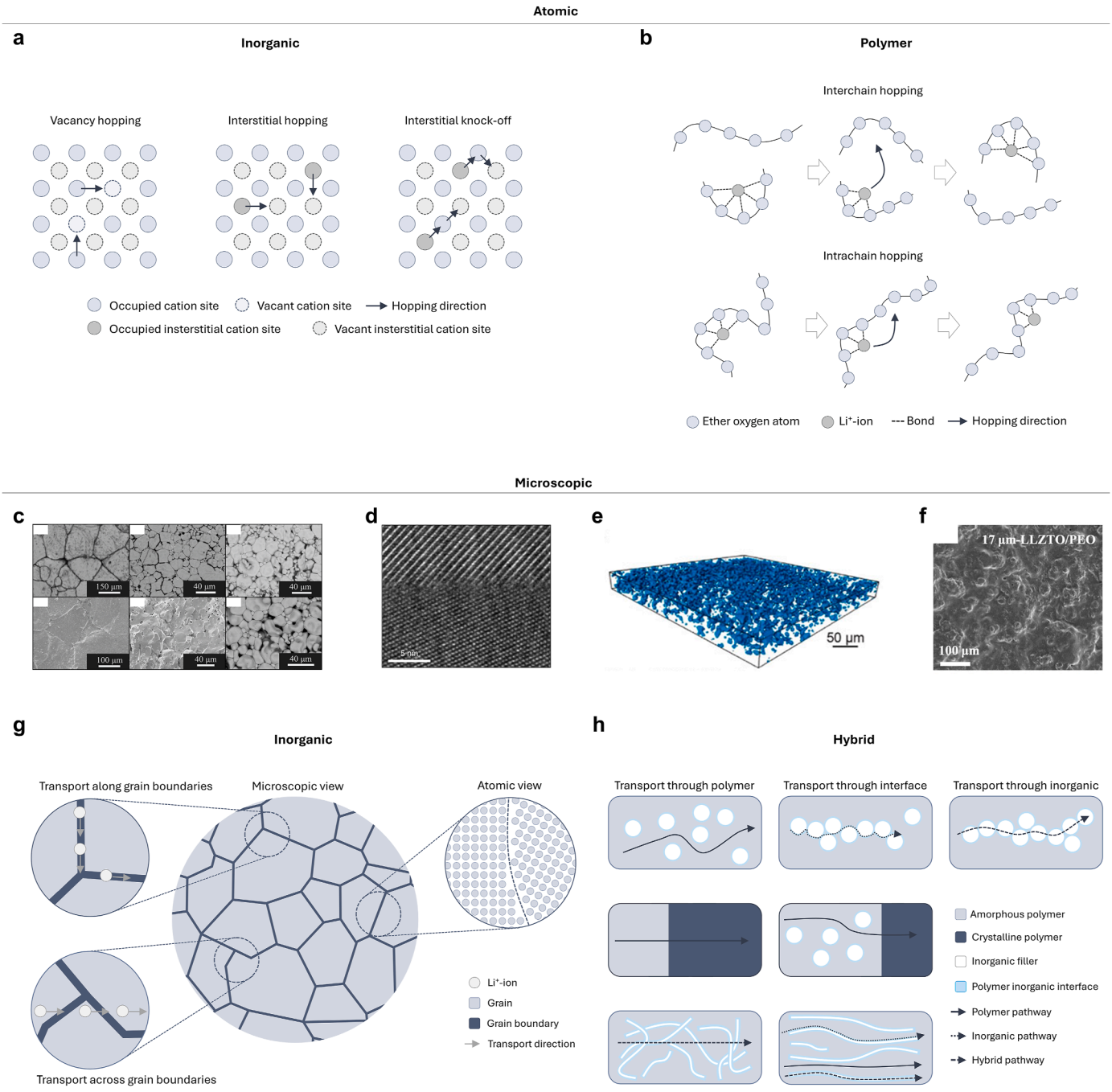

Fig. 1. Ionic transport in solid electrolytes on the atomic and macroscopic scales. (a) Ionic transport in inorganic solid electrolytes on an atomic scale. (b) Ionic transport in polymer solid electrolytes on an atomic scale. (c) SEM images of surface and cross-section morphologies of LLZO solid electrolytes sintered with different particle sizes and particle size mixtures, resulting in different kinds of grain boundaries [90]. (d) HRTEM image of a grain boundary of pristine LLZO [91]. (e) XCT scan of the filler distribution within a hybrid solid electrolyte consisting of LLZO particles in a PEO matrix [79]. (f) SEM image of the surface morphology of a Ta-substituted LLZO (LLZTO)-PEO hybrid solid electrolyte membrane [89]. (g) Possible ionic transport pathways in inorganic solid electrolytes on a microscopic scale with grain boundaries. (h) Possible ionic transport pathways in hybrid solid electrolytes on a microscopic scale with different filler morphologies and fractions.

but also can affect the quantized crystal movement (called phonons), which may act as an obstacle for moving ions. Whether and how phonons have a significant influence on the ionic conductivity is not theoretically understood yet, but the knowledge could help to improve ionic conductivity [30,31].

One of the most influential factors on the energy barrier for hopping is the crystalline structure [30]. For example, it was found that a body-centered cubic (bcc)-like anion packing structure, such as in $Li_{10}GeP_2S_{12}$ and LiP_3S_{11}, exhibits the highest ionic conductivity in comparison to other structures of similar chemistries, due to the lower activation barrier for lithium-ion hopping between the adjacent tetrahedral sites [32]. In addition to the three established ionic transportation mechanisms, several others have been proposed: ring, direct exchange, crowdion, diffusion along and across interfaces, concerted diffusion, and a paddle-wheel mechanism [25,33]. Several theoretical publications propose the use of the paddle-wheel mechanism as a possible way to improve the ionic conductivity in amorphous (glassy Li_2S–P_2S_5-based) [34] and crystalline solids (e.g., rotation of $[PS_4]$/$[SiS_4]$ polyanions in $Li_{3.25}[Si_{0.25}P_{0.75}]S_4$) [35–37]. However, it needs to be considered that the occurrence of the paddle-wheel

mechanism is always accompanied by an increase in free volume to enhance ionic transport, which cannot be properly distinguished from the paddle-wheel mechanism [38]. Like in crystals, the general ionic transport mechanism in amorphous inorganic solid electrolytes is ion hopping [29]. In particular, volume-intensive ion conduction mechanisms like the paddle-wheel mechanism are possible in the amorphous phase, which has fewer lattice interactions and therefore a lower activation energy because of the lower crystal density compared to that of a dense crystal lattice [34].

Solid polymer electrolytes, such as polyethylene oxide (PEO), are generally low ionic conductors within the range of 10^{-8} to 10^{-6} S cm^{-1} at room temperature [39]. Therefore, a solid polymer electrolyte is normally supplemented with a lithium salt to increase the ionic concentration for better ionic conductivity. Furthermore, plasticizers are often added to reduce the lower ion-conductive crystalline phase. Together with elevated operating temperatures (e.g. 60 °C), this can boost the ionic conductivities for solid polymer electrolytes up to an order of magnitude higher, from 10^{-4} to 10^{-3} S cm^{-1} [40].

While the crystalline phase in solid polymers was initially considered the major ion-conductive phase, the amorphous phase is now seen as the primary one for ion transport [41]. Later, the crystalline phase was regarded as generally a lower ionic conductive phase [42]. Nevertheless, it was found that the crystalline phases in PEO_6:$LiSbF_6$ not only can conduct ions but also exhibit even higher ionic conductivities than the amorphous phases before reaching the glass transition temperature, although the ionic conductivity is below 10^{-7} S cm^{-1} at room temperature [43].The transport mechanism was suggested to be based on cylindrical tunnels that consist of folded chains through which ions can travel. The crystalline phase usually exhibits a lower ion-conductive path. Thus, one research objective is to reduce crystallinity to achieve higher total ionic conductivities in solid polymer electrolytes [44,45].

Ion movement in a solid polymer electrolyte is predominantly a consequence of segmental motions of polymer chains in combination with bond exchanges between chain atoms and ions (Fig. 1b). Such a motion occurs more frequently above the glass transition temperature T_g, hence, materials with lower T_g offer higher conductivity [46]. Bond exchange movements are often described as hopping events, including interchain hopping between two different chains, and intrachain hopping within the same chain [47]. To break the existing bonds and create new bonds, the ions need to overcome an activation energy, similar to the ions in the inorganic crystal lattice. Hence, this process can also be described by the Arrhenius equation (1), with a pre-exponential factor A instead of the attempt frequency ν_0. Since the whole movement also depends on the polymer motion, the adapted Vogel–Tamman–Fulcher equation is introduced, $\sigma = A\exp(-B/(T-T_0))$, which takes the coupling of hopping and polymer movement into account with the experimentally measured pseudo-activation energy B and reference temperature T_0 as material-related parameters. Here, the T_0 is normally located 10–50 K below T_g and therefore is proportional to T_g [42]. Beyond linear polymers represented by PEO, polymer network electrolytes introduce an additional handle to balance conductivity and mechanical stability. In dynamically crosslinked polymers, reversible covalent motifs (e.g., imine, boronic ester, transesterification-based vitrimer chemistries) can continuously reorganize the network topology under operating conditions. This can relax local stress and heal microvoids/cracks while preserving a percolated polymer matrix for ion motion, and—when combined with plasticizers or solvating segments—can reach practically relevant conductivities without relying solely on a highly crystalline/soft phase [48–50].

In contrast to inorganic solid electrolytes, solid polymer electrolytes usually conduct both cations and anions. This leads to a transference number that is usually significantly lower, thus lowering the actual lithium-ion conductivity of the solid polymer electrolytes [51].To address this, single-ion conducting polymer electrolytes raise the lithium-ion transference number by immobilizing anions that are present on the polymer backbone by synthetic design. The concentration polarization is thereby lowered through the depletion of lithium ions and the accumulation of counterions, and excessive accumulation of the SEI from anion and polymer reduction is also reduced, both of which are critical factors that can otherwise amplify interfacial non-uniformity during electrodeposition [52–56].

3. Ionic transport on a microscopic level

Because inorganic solid crystalline electrolytes are not normally monocrystalline—i.e., only isotropic in a short range—the occurrence of interfaces between differently oriented grains and/or different crystal structures, namely grain boundaries (Figs. 1c and d), is not negligible when discussing their ion transport. Hence, ions need to either cross or move along the grain boundaries to traverse a solid electrolyte on the microscopic scale, so a modified transport mechanism needs to be assumed [25,57]. Beneficial techniques to uncover material microstructures, such as grain boundaries in inorganic solid electrolytes (Figs. 1c and d) or filler distributions in hybrid solid electrolytes (Figs. 1e and f), are scanning electron microscopy (SEM), transmission electron microscopy (TEM), or high-resolution transmission electron microscopy (HRTEM). To characterize the ionic transport within solid electrolytes and at interfaces to link to their microstructures, various methods can be employed [58]. Typically, electrochemical impedance spectroscopy (EIS) is used to measure the ionic conductivity within a broad frequency range (mHz to MHz) and on large length scales (10^{-7}–10^{-2} m). Beside determining bulk ionic conductivities, EIS is able to distinguish between bulk, interface, and grain boundary contributions [59]. However, measuring ionic hopping across individual grain boundaries remains technically challenging due to high contact resistances, which require four-point probe setups. For smaller length scales (10^{-11}–10^{-7} m), the diffusion coefficient of ions can be determined with nuclear magnetic resonance (NMR). This technique can be utilized to investigate ionic hopping between different phases, such as inorganic and organic ones in hybrid solid electrolytes.

Due to morphological and electrochemical changes at the grain boundaries, new energetically favorable pathways can occur (Fig. 1g). Via molecular dynamic simulation, it was found that lithium-ion transport in LLZO at the grain boundary region is generally slower compared to in bulk regions [60]. In agreement with that, it was reported that the grain-boundary ionic transport of lithium aluminum titanium phosphate (LATP) is three orders lower than through the material's bulk [61]. As a consequence, lithium ions were found to move preferentially through the grains instead of along the grain boundaries [62]. However, the difference is highly dependent on temperature and the orientation of grains to each other [60]. Larger angles of misorientation between grains result in an increase in grain boundary energies [63], where a low grain boundary energy is correlated with the presence of a high grain boundary density, which, in turn, causes high ionic resistance and thus, lower ionic conductivity [57]. Nevertheless, grain boundaries do not always lower ionic diffusion. Theoretical calculations reveal that in some oxides, such as HfO_2 [64], grain boundaries enhance ionic transport. Moreover, Wilkening et al. [65] found enhanced ionic conductivity in the nanocrystalline phase of $LiNbO_3$, which was attributed to the amorphous interfaces between different crystals because the more disordered structure facilitated ion transport [66]. The reason for the increased ionic conductivity in certain glass ceramics, such as Li_3PS_4, is not yet known [67]. Typical ionic conductivities of different inorganic solid electrolytes can reach from 10^{-7} to 10^{-2} S cm^{-1} at room temperature [18]. Furthermore, the presence of pores within inorganic solid electrolytes increases the diffusion tortuosity, which leads to lower effective transfer efficiency and inhomogeneous ionic current distribution. The elimination of pores within the solid electrolyte always favors the solid electrolyte's application.

Hybrid solid electrolytes consisting of solid inorganic (represented as the filler) and organic (represented as the matrix) parts provide promising design approaches for improving solid electrolyte properties [68,

69]. This method is based on combining the promised advantages of inorganic conductors, such as high ionic conductivity and thermal stability, with the benefits of organic ionic conductors, such as high mechanical flexibility and good compatibility with electrode materials [23, 70]. While an active filler potentially contributes to the ionic conductivity by providing new pathways through the filler phase, a passive one does not conduct ions. Yet, a passive filler can also increase the ionic conductivity in a hybrid solid electrolyte by impeding the crystallization of the polymer phase [71], lowering its glass transition temperature, aiding lithium salt dissociation, and/or reducing the hopping energy [72–74]. Other important filler properties that affect the ionic and mechanical properties of a hybrid solid electrolyte are its quantity (number of single filler parts), size (e.g., diameter), shape, and distribution, and the orientation of the used filler.

Regarding ion transport in hybrid ionic conductors, three different pathways are proposed: inside the polymer, inside the inorganic part (active filler), and along the interface between the polymer and the inorganic filler (Fig. 1h). Which pathway the ions prefer seems to depend heavily on the specific characteristics of the hybrid solid electrolyte system. Even the use of the same filler, such as LLZO, leads to different conclusions. As a result, reports in the literature are somewhat contradictory [70]. Based on NMR active isotope tracking, Zheng et al. [75] proposed the ceramic phase as the main pathway for 50 wt% (i.e. 18 vol%) LLZO particles in a PEO-$LiClO_4$ system. In contrast, Chen et al. [76] reported that the suppression of PEO crystallinity through incorporating LLZO particles increased conductivity, based on differential scanning calorimetry measurements. This, in turn, would suggest that the amorphous polymer phase is the main conductive phase. In addition to experimental data, theoretical calculations also suggest that lithium-ion transport takes place primarily along the interface between $LaCoO_3$ nanofibers and PEO [77]. For hybrid solid electrolytes made with lithium lanthanum titanium oxide (LLTO) ceramic nanofibers in a polyvinylidene fluoride–hexafluoropropylene (PVDF-HFP) matrix, NMR disclosed that lithium ions are using all three possible pathways, leading to a higher ionic conductivity and lithium-ion transference number [78]. Nevertheless, the conductivity enhancement achieved by adding fillers to hybrid solid electrolytes seems to be limited by increasing tortuosity in the lithium-ion pathways (when assuming they travel only through a single phase) [70] and the hindering of segmental motion due to the high volume fraction of fillers [79]. This, in turn, implies that lithium ions seem not to hop between the ceramic and polymer phases. Accordingly, there is a certain filler content at which the ionic conductivity goes from improved to deteriorated [80]. For example, 10 wt% LLZO in PEO exhibits a lower crystallinity than 0 wt% and 20 wt% LLZO in PEO [79]. That 10 wt% LLZO in PEO results in higher conductivity than the other two supports the theory that the amorphous polymer is the main conducting path for lithium-ion transport.

In general, whether the ionic conductivity is improved in hybrid solid electrolytes depends on the interplay of filler content, ionic conduction in each phase, and filler orientation and distribution. For instance, if the inorganic phase exhibits a higher ionic conductivity than the polymer one, the amount of filler needs to be large enough to create a continuous percolation path or must be significantly more ionically conductive to compensate for the higher energy path inside the polymer and across the interface. For the LLZO commonly used in PEO composites, it is reported that a high activation energy creates a highly resistive interface, making the interfacial crossing energetically unfavorable [81]. Furthermore, an inorganic pathway is always necessarily intertwined with ions crossing the interfaces between individual filler parts, except for nanofibers aligned from one end to the other. Liu et al. [82] stated that the interface between PEO and LLTO nanofibers presents a highly ionic conductive pathway, resulting in even higher ionic conductivity with aligned nanofibers due to reduced tortuosity. Because of the different processes taking place in hybrid solid electrolytes, it is difficult to distinguish between the different mechanisms leading to the final enhanced ionic conductivity. Frequently, researchers propose a combination of several mechanisms to explain an ionic conductivity increase observed experimentally [83,84]. Likewise, modeling the ionic conductivity of hybrid solid electrolytes can become complicated. Similar to polymer and inorganic solid electrolytes, the general ionic conductivity of a hybrid solid electrolyte follows the Arrhenius equation (1), including a pre-exponential factor with a proportional dependency on the carrier concentration [80]. Depending on the pathway, the activation energy within the hybrid solid electrolyte differs between the polymeric, inorganic, and interface phases. Therefore, when using several phases, a hybrid solid electrolyte displays an average conductivity rather than an isotropic one. In general, ionic conductivities of different solid polymer electrolytes can be improved with ceramic fillers up to 10^{-3} S cm^{-1}, but commonly only to 10^{-4} S cm^{-1} at room temperature or slightly elevated ambient temperatures (30–60 °C) [85–88]. Since the filler orientation and content seem to be decisive, too, the general distribution of fillers needs to be considered. Inhomogeneous distribution could impact the ion conduction behavior and induce batch-to-batch ionic conductivity variation in solid electrolytes. Via X-ray computed tomography (XCT), the distribution of filler within a polymer or vice versa can be studied, as was shown by Din et al. [79], who revealed uniformly distributed LLZO particles inside a PEO-based polymer matrix (Fig. 1e). The filler size influences the roughness of the surface as well, which further affects the interfacial contact between solid electrolyte and electrode. This can be investigated by SEM (Fig. 1f) as well as atomic force microscopy [89]. Owing to the larger diameter of filler particles, an increased surface roughness between the hybrid solid electrolyte and the electrode is observed, which, in turn, increases the interfacial resistance, due to inhomogeneous contact.

4. Homogeneous plating and stripping

The reactions at the anode represent the reduction from a lithium ion to a lithium atom during plating, and oxidation from a lithium atom to a lithium ion during stripping. For both processes, the lithium metal needs to conduct electrons to or from the solid electrolyte/lithium metal interface. Because lithium exhibits a high electronic conductivity of ~100 kS cm^{-1}at room temperature compared to the nine-magnitudes-lower ionic conductivities of solid electrolytes [92], the current of the electrons in a battery depends on the current of the lithium ions. If the electronic current is much higher than the ionic one, negative charges build up at the anode side during charging, raising the potential energy to overcome further electron accumulation. This leads to a self-regulating mechanism limiting the global electronic current in the case of a uniformly lower ion current. Hence, the ionic conductivity of the solid electrolyte is the bottleneck for fast charging in an idealized system; in other words, to preserve uniform lithium metal deposition, the ion flux needs to be equal to the magnitude of the electron flux everywhere at the interface.

Homogeneous lithium plating and stripping are highly affected by defects at the interface between the solid electrolyte and the lithium anode, such as impurities, pores, cracks, flaws, and grain boundaries. In most solid polymer electrolytes, both lithium ions and anions move freely due to ion transport based on the polymer's segmental motion. Homogeneous lithium plating and stripping are possible under a low current density, where ionic concentration evolves to a steady state with a constant concentration gradient in the solid polymer electrolyte. Once a high current density is applied, lithium ions at the solid electrolyte/anode interface are rapidly deposited into lithium atoms, while anions move rapidly to the cathode side. This drastic ionic concentration difference creates a large electric field and forms a space charge at the interface between the lithium anode and the solid electrolyte, favoring dendrite growth, i.e., Sand's time [93]. Thus, increasing the lithium-ion transference number by incorporating ceramic fillers, or developing single-ion polymers utilizing the covalent bond between the anion and the polymer backbone to immobilize the anion, have proved that stable lithium plating and stripping can be achieved at relatively high current densities [52].

Unlike solid polymer electrolytes, the ion transport mechanism for inorganic solid electrolytes is based on single-ion conduction, which avoids concentration gradients within the solid electrolyte during battery operation. However, how the lithium-ion transport mechanism in inorganic solid electrolytes affects lithium plating and stripping has received little attention, due to the difficulty of directly observing lithium plating and stripping between the rigid inorganic solid electrolyte and the lithium anode or current collectors, since SSLBs often operate under high external pressure in the MPa range. Nevertheless, research on how the SEI in cells with liquid electrolytes affects lithium deposition provides this insight: solid electrolytes with high relative density and higher conductivity that avoid diffusion-controlled processes during lithium deposition—which evade dendritic lithium formation via a diffusion–reaction competition mechanism—are favorable [94]. However, liquid electrolytes enable ionic transport across the entire anode volume, allowing the development of various lithium morphologies, depending on the operating conditions. By contrast, solid electrolytes restrict lithium deposition to a two-dimensional interface, thereby promoting the formation of dense lithium grains, especially at elevated operating pressures. Recently, Fuchs et al. [95] used a combination of focused ion beam and electron backscatter diffraction to reveal the grain size and orientation of deposited lithium, using $Li_{6.5}Ta_{0.5}La_3Zr_{1.5}$, Li_6PS_5Cl, and $Na_{3.4}Zr_2Si_{2.4}P_{0.6}O_{12}$ (Na-ion conductor) as solid electrolytes. The results suggest that the properties of solid electrolytes and current collectors may not be the crucial factors influencing metal anode plating and stripping. Therefore, the lithium-ion conduction mechanism may not play a critical role once the diffusion of lithium ions can reach a certain threshold for avoiding dramatic polarization or space charge at interfaces, and the microstructure of the lithium metal anode is the decisive factor.

Without any external impacts, bulk lithium crystallizes in a bcc crystal lattice at room temperature [96]. Yet, it was reported that in the presence of a solid electrolyte, lithium crystallizes via a multiple-step pathway during charging [97]. According to theoretical calculations, lithium first nucleates in a disordered arrangement, followed by a random hexagonal close-packed crystal structure, and finally in the bulk bcc structure, based on the assumption of a Li_2O interlayer between the anode and the solid electrolyte. Similarly, the process takes place in a liquid electrolyte consisting of two interdependent reduction and electrocrystallization steps [98]. Like inorganic solid electrolytes, lithium metal is composed of grains whose morphology is affected during lithium plating (grain coarsening) and stripping (pore formation) [95]. Utilizing cryogenic TEM and molecular-level simulation, it was shown that initial lithium nucleation is dependent on atomic interactions, such as atom packing density and energy transfer, which determine the occurrence of ordered or disordered nanostructured lithium nucleation [99].

Commonly used cathodes in a solid-state battery, such as lithium cobalt oxide (LCO) and lithium nickel manganese cobalt oxides (NMC), store lithium ions via intercalation, which is accompanied by volume expansion (LCO) or contraction (NMC) under charging, and vice versa during discharging [100,101]. Depending on the volume change of the battery stack, the cathode either expands, leading to better contact or higher stress, or contracts, leading to contact loss or lower stress. While expansion/contraction within the plane of the cathode only affects the cathode itself, expansion in the stack direction acts along the battery stack. While the first row of lithium atoms at the interface strips off, the solid electrolyte needs to move toward the anode (driven by stack pressure, the total stack thickness decreases), or new lithium atoms need to migrate to the interface to preserve the contact. The latter can occur either by lithium atoms moving through the lithium metal towards the interface (self-diffusion), or by the mechanical creep of lithium. To preserve globally uniform stripping, the local ion flux needs to be consistent across the whole interface, which depends on the sufficient replenishment of lithium atoms for oxidation through lithium creep or self-diffusion. If lithium atoms move without pressure via diffusion to the interface, the self-diffusion coefficient of lithium, which is mostly observed within the magnitude of 10^{-11} cm^2 s^{-1}, becomes decisive [102]. In the case of a solid electrolyte with a high lithium-ion diffusion coefficient (for example, 10^{-9} cm^2 s^{-1} for LLZO [102]) and the high electronic conductivity of lithium metal, the lithium self-diffusion process will present as the limiting factor for fast discharging. However, Kasemchainan et al. [103] reported lithium creep as the predominant transport mechanism from lithium to a Li_6PS_5Cl/Li interface stacked with a sufficient pressure in the MPa range. Lithium is prone to experience creep deformation under tension or compression because of its low melting temperature (180.5 °C), with dislocation climb as the dominant creep mechanism at room temperature [104]. As the strain rate is proportional to $e^{-1/T}$, lithium creep increases at higher temperatures. Nevertheless, Ding et al. [105] show that the compressive creep deformation rates of lithium are typically in the order of a few μm h^{-1} under an applied pressure of 0.6–3.6 MPa at ambient temperatures, which could have a pronounced effect during storage or long-term practical use. Given the circumstances, it becomes obvious that a temporally and locally uniform replenishment (stripping) and uniform plating of lithium at the interface are crucial for maintaining homogeneous contact (Fig. 2a).

5. Electrochemical potential

Electrochemical potential, a combination of chemical potential and electrical potential, is a crucial parameter for understanding the movement of charged particles like ions and electrons, especially in battery systems. In a thermodynamic equilibrium, the open circuit voltage V of a battery cell is defined as $V = (\mu_{Li,A} - \mu_{Li,C})/eF$, where $\mu_{Li,A}$ and $\mu_{Li,C}$ are the chemical potential of lithium in the anode and cathode, respectively, F is Faraday's constant, and e is the elementary charge. This relation is a consequence of the electrochemical potential $\tilde{\mu}$, which is a constant number in an equilibrium state [106,107]. The chemical potential of lithium consists of $\mu_{Li} = \mu_{Li^+} + \mu_{e^-}$, i.e., the summed chemical potentials of lithium ions μ_{Li^+} and electrons μ_{e^-} in the considered area (Fig. 2b) [108]. Because of the high reduction potential of lithium in the anode and relatively high oxidation potential of lithium ions in the cathode, plus the electron-insulating property of the solid electrolyte, the electrochemical potential of electrons drops significantly from the anode to the cathode. As a result, ions accumulate in the solid electrolyte and electrons accumulate in the anode at the solid electrolyte/anode interface, and vice versa at the cathode side. To balance this space charge layer, an electrical potential Φ builds up. Ultimately, this defines the electrochemical potentials of the charge carriers as $\tilde{\mu}_{Li^+} = \mu_{Li^+} + F\Phi$ and $\tilde{\mu}_{e^-} = \mu_{e^-} - F\Phi$. Since the solid electrolyte and both electrodes are ionically conductive, $\tilde{\mu}_{Li^+}$ is constant, and thus, μ_{Li} corresponds to the course of $\tilde{\mu}_{e^-}$. However, given its thickness is in the nanometer range, the space charge layer is regarded as both negligible and crucial for the performance of solid-state batteries, contingent upon the interface and the voltage difference at the interface. For the interface of LLZO/LCO, de Klerk et al. [106] found that the space charge theoretically caused a resistance below 1 Ω cm^{-2}, which they thus designated as negligible when simulating a cell voltage up to 4.3 V vs. Li/Li^+. In contrast, Katzenmeier et al. [109] suspect that the space charge layer explains the degradation occurring at the interface between lithium anodes and solid electrolytes.

6. Microscopic failure mechanism characterization

The previously considered concepts assume idealized conditions, such as perfect macroscopic crystals, with perfect interfaces and without unwanted chemical reactions, which result in uniform plating and stripping. In addition, they do not factor in the effects of pressure changes arising from volume expansion, side product generation, or applied battery stack pressure. In reality, the nucleation and propagation of dendrites or lithium filaments are some of the severe consequences

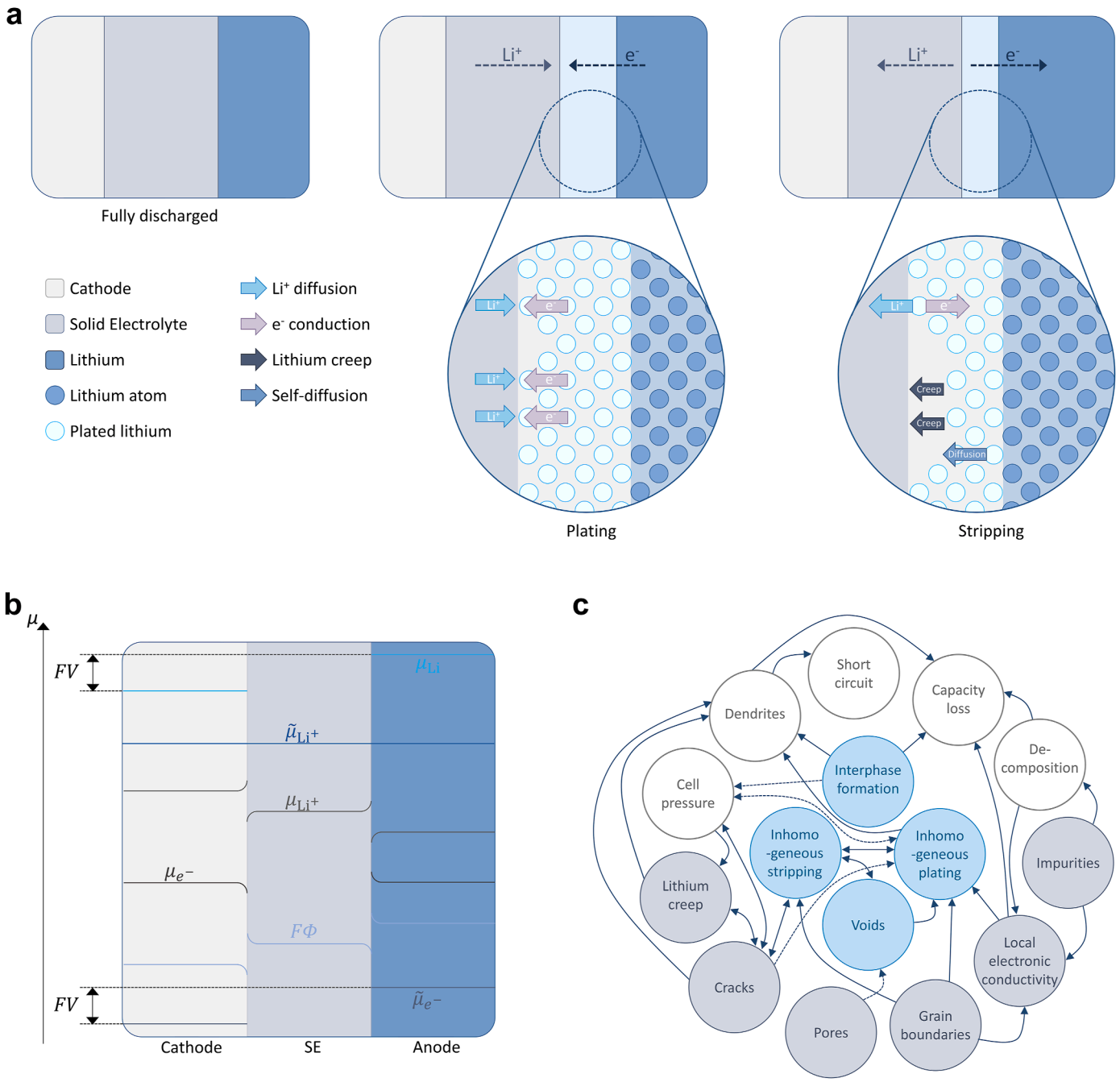

Fig. 2. Schematic illustrations of different fundamental occurrences in solid-state lithium metal batteries. (a) Illustration of the plating and stripping process of a lithium metal anode with a solid electrolyte, incorporating lithium-ion diffusion, electron conduction, lithium creep, and lithium self-diffusion. (b) Progression of the chemical potential μ and electrochemical potential $\tilde{\mu}$ in an electrochemical equilibrium for lithium ions and electrons (adapted from Ref. [108]). (c) Physicochemical entanglement of origins, cycling consequences, and cell consequences for different degradation mechanisms. The arrow direction indicates the direction of action. Light blue highlights the interface and blue-gray the solid electrolyte as the location of action.

arising from these undesirable processes during cycling. Microscopic techniques such as XCT, SEM, and TEM can be gainfully utilized for imaging degradation mechanisms in solid-state batteries (Table 1) [110–112]. However, despite the useful impact of microscopes, the possible influence of radiation always needs to be considered. For example, it has been found that lithium metal growth kinetics and morphology are significantly altered by an electron beam [113].

X-ray computed tomography (XCT) is a powerful method to image an object's internal microscopic structure. Illuminating a rotating sample with X-rays and detecting the radiation that passes through the sample leads to two-dimensional absorption patterns for multiple orientations. The absorption pattern is determined by the attenuation of intensity, which is dependent on the path length and the mass attenuation coefficient (dependent on the X-ray energy) of the penetrated material/element. Reconstruction based on the captured two-dimensional projections creates cross-sectional images, which can be compiled into a three-dimensional image of the sample.

XCT provides a three-dimensional reconstruction, whereas SEM only investigates the surface, and TEM creates a two-dimensional projection of a thin three-dimensional layer. In addition, XCT is regarded as non-destructive, enabling *in operando* measurements on a cell level. This may be a key advantage for the further development of batteries, since it

Table 1
Different microscopy techniques for studying solid-state lithium metal batteries.

Technique		Operation and capabilities	Challenges
X-ray computed tomography	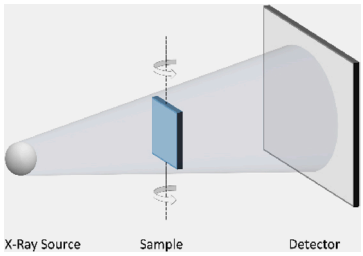	X-rays penetrating through a rotating sample, resulting in an absorption pattern on the detector Key properties: • Three-dimensional morphological characterization • Sub-micrometer range • Non-destructive • *In operando* • Lab based or synchrotron	• Low resolution compared to electron microscopy • Long scanning time for 3D scans • Low visibility of lithium • Possible beam damage • Suitable XCT cells
Scanning electron microscopy	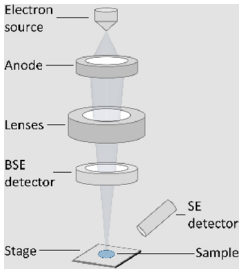	Electron beam is focused on a sample, resulting in either detected secondary or backscattered electrons from the sample surface Key properties: • Nanometer range • Surface morphological characterization • Cryogenic compatible	• Requires electronically conductive sample (or surface) • Investigation in high-vacuum environment • Possible beam damage • No wet/liquid samples
Transmission electron microscopy	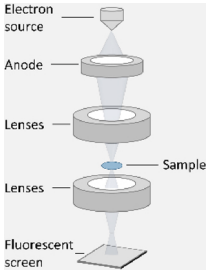	Electron beam is focused on a sample and penetrates it, resulting in an intensity pattern on the fluorescent screen Key properties: • Sub-nanometer range • Projection of three-dimensional on two dimensions • Cryogenic compatible	• Requires electronically conductive sample • Investigation in ultra-high vacuum environment • Sample needs to be thin (< 100 nm) • Possible beam damage
(Cryogenic) focused ion beam tomography	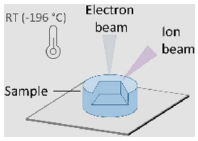	Ion beam removes layer by layer of a sample while an SEM image is taken after each layer. Key properties: • Three-dimensional morphological characterization • Nanometer range • Cryogenic compatible	• Destructive • Requires electronically conductive sample or surface for SEM • Investigation in high-vacuum environment

can visualize the complete degradation process instead of just one intermediate or post-mortem state. However, XCT offers only a limited resolution, which is in the sub-micrometer range for micro XCT scanners and the tens of nanometers (~50 nm) for nano-XCT. While micro-XCT devices are usually capable of scanning a whole cell (e.g., coin cells [114] or pouch cells [115]), nano-XCT devices are further limited with respect to sample size, making *in operando* measurements difficult. The cell design for *in operando* measurements is another demanding factor, due to necessary conditions such as air tightness, low-absorbing cell materials, and small but easily assembled housing [116]. Based on the notably higher photon flux, the usage of synchrotron radiation reduces the measuring time and can enhance the image quality significantly compared to laboratory XCT scanners. Reducing the measuring time, which is usually a few hours (2–5 h) for sufficient image quality scans, is one key factor for improving *in operando* experiments. One further challenge for investigating lithium metal batteries with XCT is the weak interaction between X-rays and lithium atoms. Especially next to highly attenuating materials, such as current collectors made of heavy elements (e.g., Cu), lithium is hardly visible, and difficult to distinguish from voids. To overcome this issue, a phase contrast mode can be utilized to enhance the edge contrast between lithium metal and its environment [117–119]. For laboratory XCT scanners, phase contrast can be implemented with a propagation-based phase contrast by increasing the source-to-sample and sample-to-source distances, but it comes with decreased photon flux, making longer scans necessary to maintain a sufficient signal-to-noise ratio [116,120].

The biggest advantage of scanning electron microscopy (SEM) is the high resolution in the nanometer range, paired with a relatively easy measurement procedure. This technology is realized by emitting an electron beam that interacts with the surface atoms of the sample, which can provide structural and compositional information by detecting the secondary or backscattered electrons. Insulating samples need to be coated with an electronic conductor or measured under highly restricted current and voltage settings to avoid charge accumulation and achieve sufficient image quality. Electronic conductive samples can be measured without any preparation. SEM measurement provides real-time visualization of dynamic evolution—for example, lithium filament growth by e-beam or tip manipulation [121], void formation, followed by void merging [122], or lithium metal fatigue [123]. Morphological evolution can be monitored *in operando* to uncover the failure mechanisms resulting from lithium dendrite formation. Although *in operando* measurements offer valuable insights into battery cycling behavior, comparability with normally used cells must always be ensured, especially when considering exposure to high-vacuum environments and possible damage from the electron beam. Furthermore, SEM measurements performed without applied stack pressure can result in a significantly different cell setup compared to commonly used cells. To overcome the resolution limitations of XCT, focused ion beam (FIB)-SEM tomography can be performed. This technique enables high-resolution three-dimensional image reconstruction but is destructive. For organic samples, cryogenic FIB devices are necessary to avoid damaging the polymer. It can also be used for precisely determining solid-electrolyte

porosity, which is correlated to ionic conductivity and dendrite growth [124,125]. For beam-sensitive materials or interfaces, cryogenic SEM devices are necessary to avoid damaging or altering the region of interest [126].

TEM offers the highest resolution, from the nanometer to the atomic scale. On the atomic scale, it enables the gathering of precious information, particularly about atomic migration/transportation, reaction kinetics, local chemical information, and micro-/atomic-structure evolution. By emitting high-energy electrons that pass through a thin sample, an image of the sample can be formed from the interaction of the incident electrons with the atoms of the sample. It also provides real-time, dynamic monitoring of the failure mechanisms and electrochemical reactions for battery materials. However, sample preparation is difficult because samples with a thickness of less than 100 nm are necessary. FIB and ultramicrotomy sample preparation are typically used. As with SEM samples, TEM samples should be electronically conductive and may be damaged by the high-energy electron beam. The measurement needs to be conducted in an ultra-high vacuum environment, which makes electron microscopy unsuitable for wet or liquid-containing samples. While diffraction contrast tomography can be performed with XCT scanners, SEM and TEM offer convenient combination measurements with spectroscopy, scattering, and mass-spectroscopy-based techniques such as energy dispersive X-ray spectroscopy, electron energy loss spectroscopy, etc. Like SEM, TEM can be performed at cryogenic temperatures, enabling the investigation of beam-sensitive materials, such as polymers, as well as interfaces [126].

All of the foregoing microscopy techniques require airtight, non-destructive, and non-altering sample preparation and transfer. Because the investigation demands a vacuum environment, TEM and SEM measurements require airtight transfer from the inert atmosphere to the device. For that, commercially available airtight transfer chambers can be used. In contrast, XCT measurements are conducted in ambient air, making continuous, sample-adapted air protection for the sample necessary. For postmortem or material characterization, simple embedding with solvent-free polymers such as epoxy can be utilized for temporary sealing. Here, damage- and alteration-free preparation of the region of interest always needs to be ensured.

To overcome the individual limitations, such as the low resolution of XCT or the destructiveness of FIB-SEM, individual microscopy techniques can be combined in a correlative approach, enabling highly advanced and enlightening microscopic characterization. A promising approach is combining a high-field-of-view, three-dimensional XCT scan for region of interest localization with a subsequent FIB-SEM high-resolution measurement of the selected area [127]. Even more insightful, but also demanding, is a preceding *in operando* XCT experiment, with a subsequent high-resolution FIB-SEM measurement to gain microscopic information about the pristine state and its development over time. Especially for dendrite mechanism analysis, correlative microscopy can play a key role in overcoming the problem of resolving sub-micrometer dendrites with XCT and displaying only one surface with SEM, by using complementary measurement techniques.

Besides the foundational microscopy techniques thus far introduced (XCT, SEM, TEM), other advanced techniques such as acoustic diagnostics or neutron depth profiling (NDP) are utilized for advanced *in operando* characterization of SSLBs. For detailed information about more techniques for electro-chemo-mechanical measurements, we refer readers to other review articles [128–130].

7. Critical plating

Originating from local chemical, mechanical, or physical deviations, non-uniform plating and stripping of lithium result in unwanted filament growth inside the solid electrolyte or at the solid electrolyte/anode interface (Fig. 2c). Once the electronic or ionic current at a certain point deviates from the rest of the interface, non-uniform plating and stripping occur.

The current density is commonly regarded as one of the main quantities to define a threshold for dendrite growth. Until a critical current density (CCD) is reached, plating without cell failure due to dendrites is possible. Inorganic solids can reach CCDs of > 1 mA cm^{-2} but are mostly lower than 10 mA cm^{-2}. Polymer and hybrid solid electrolytes exhibit CCDs mostly lower than 1 mA cm^{-2}, while some are reported to reach up to 5 mA cm^{-2} [102,131]. According to the ionic transport mechanism, higher temperature improves the diffusivity of ions in the solid electrolyte as well as lithium atoms in the lithium anode, and therefore the CCD [102]. However, when determining the CCD, one assumes the whole electrode surface to be a current-conducting area, without consideration of the actual connected areas (i.e., effective connected area). For example, voids at the solid electrolyte/electrode interface result in higher local current densities than the average current density. Consequently, the local current densities can surpass the assumed average current densities by many times, weakening the meaningfulness of the CCD. For this reason, Jiao et al. [132] proposed the theoretically determined local current density (LCD), and Klimpel et al. [133] proposed a standardization for CCD measurements. While the first is only based on simulation, the second relies on experimentally measuring the areal capacity limitation. Both concepts propose to evaluate the dendrite growth via current densities but with consideration of the local current density variance and current distribution, respectively. With the CCD as a criterion for dendrite growth or battery failure, it is important to note that the current density itself is not the origin of battery failure. It is only the point at which the current amplifies inhomogeneous plating and stripping to an extent that is harmful to the cell. Since it is also not generally defined how long the critical current needs to be applied, the CCD is highly dependent on the plating time, i.e., the areal capacity. Therefore, using areal capacity instead of CCD can improve the comparability and expressiveness of battery performance tests, as Morchhale et al. [134] discussed regarding argyrodite solid electrolytes. For commercial relevance, areal capacities of > 3 mAh cm^{-2} at current densities of > 3 mA cm^{-2} need to be achieved [135]. As illustrated in Fig. 2c, inhomogeneous plating, while being one cause of dendrite or filament growth, is always a consequence of local discontinuities like grain boundaries, interphases, voids, pores, or cracks inside the cell components and interfaces.

8. Voids and critical stripping

Under realistic circumstances, taking the morphology of the solid electrolyte/electrode interface into account leads to an often-reduced interfacial contact area due to surface defects, such as flaws, impurities, and pores or uneven surfaces. While voids are characterized as missing contact points at the electrolyte/electrode interface, pores refer to material free volume inside the bulk or at the surface as a property of the electrolyte. To overcome contact issues, inorganic solid electrolytes are commonly cycled under very high external stack pressure to support lithium creep inside the voids [136,137]. However, too high a stack pressure can harm the cell. On the one hand, it was found that a Li/L-i$_6$PS$_5$Cl/NCA battery can undergo more than 200 cycles at room temperature with a stack pressure of 5 MPa, while the battery shorts after a short time at 25 MPa, and immediately at 75 MPa [138]. On the other hand, stable cycling for 100 cycles at considerably higher applied operation pressures is reported for an In–Li/ß-Li$_3$PS$_4$/LCO battery with 70 MPa at 25 °C [139].Even for 191.07 MPa at 60 °C with a Li–In/Li$_6$PS$_5$Cl/NCM battery, stable cycling for > 100 cycles is possible [140]. One reason for the widely disparate stack pressure values could be the different pressing pressures of the individual components during cell assembly. Here, the solid electrolyte was pressed by hand [139], with 200 MPa [140], and with 370 MPa [138]. Similarly, the cathode–solid electrolyte–anode stack was pressed with different pressures: 120 MPa (LiIn anode, 25 MPa for Li anode) [138], 0.29 MPa (In–LiIn anode) [139], and 100 MPa (LiIn anode) [140]. This may have led to the

solid electrolyte having significantly different densities and porosities before the application of stack pressure for cycling. For a lower stack pressure, lithium crept only in the voids at the solid electrolyte/electrode interface. However, XCT revealed that lithium had also crept inside the pores of a Li_6PS_5Cl electrolyte to form dendrites at higher stack pressure (Fig. 3a) [138].The long-term sustainability of applying high external pressure to a battery cell without affecting the physical properties of the lithium electrode and solid electrolyte is not yet clear.

Another possible approach to maintain uniform interfacial contact is based on increasing the cell operational temperature for enhanced lithium atom self-diffusion and creep [137,141]. This approach was extended to a significantly elevated temperature by Jin et al. [142], who utilized a temperature of 240 °C to obtain a molten lithium anode, which eliminated the dependency on lithium self-diffusion and creep for achieving good interfacial contact with a LLZTO electrolyte. In general, it was shown that changing from solid to molten lithium is connected to a step increase in CCD, with LLZO as high as 1100 mA cm^{-2} [143]. But besides the additional benefit of improved ionic conductivity, increasing the temperature requires energy, which lowers the battery energy efficiency. Moreover, it introduces an additional complexity for commercial cells. A similar approach is to use GaInSn, a liquid metal alloy at room temperature, as an interlayer between a Li_6PS_5Cl electrolyte and a lithium anode to enhance the interfacial contact [144]. With the interlayer approach, it is important to note that the alloying/dealloying of lithium during charge/discharge can transform the alloy phase from liquid to solid through eutectic transformation.

Compared to inorganic electrolytes, a distinctive advantage of polymeric electrolytes is the potential to continuously restore interfacial contact to repair void-induced contact loss. For example, self-healing, dynamically crosslinked polymers bearing reversible motifs (e.g., H-bond, imine, boronic ester) can continuously reorganize the polymer network by breaking and reforming the crosslinking sites under operating conditions. This property allows a complementary mechanism to relax local stress and heal voids while maintaining ionic motion [50, 145–148].

Another factor is relevant to cell cycling dynamics. Even when initial contact between the solid electrolyte and the electrode involves no voids, contact loss can arise during cycling. If the stripping current is locally higher than in other areas at the solid electrolyte/electrode interface (e.g., due to impurities), vacancies can accumulate at the interface, ultimately forming voids [149]. Accordingly, it was found that the vacancy diffusion inside the lithium metal is a decisive factor for stable stripping under a high anodic load with LLZO electrolyte [150]. The self-diffusion of lithium atoms to the interface can be considered lithium vacancy diffusion into the lithium anode, and vice versa. Commonly, the CCD is associated with dendrite growth that occurs during plating [103]. However, high currents during stripping can also lead to altered surfaces, which, in turn, favor dendrite growth during subsequent lithium deposition. The CCD for stripping is the current density at which the void formation is so severe that the resistance, and thus the potential, rise drastically, followed by uncontrolled dendrite growth in the subsequent plating cycle, or in the same cycle in symmetric lithium metal cells [151]. This explains the importance of the

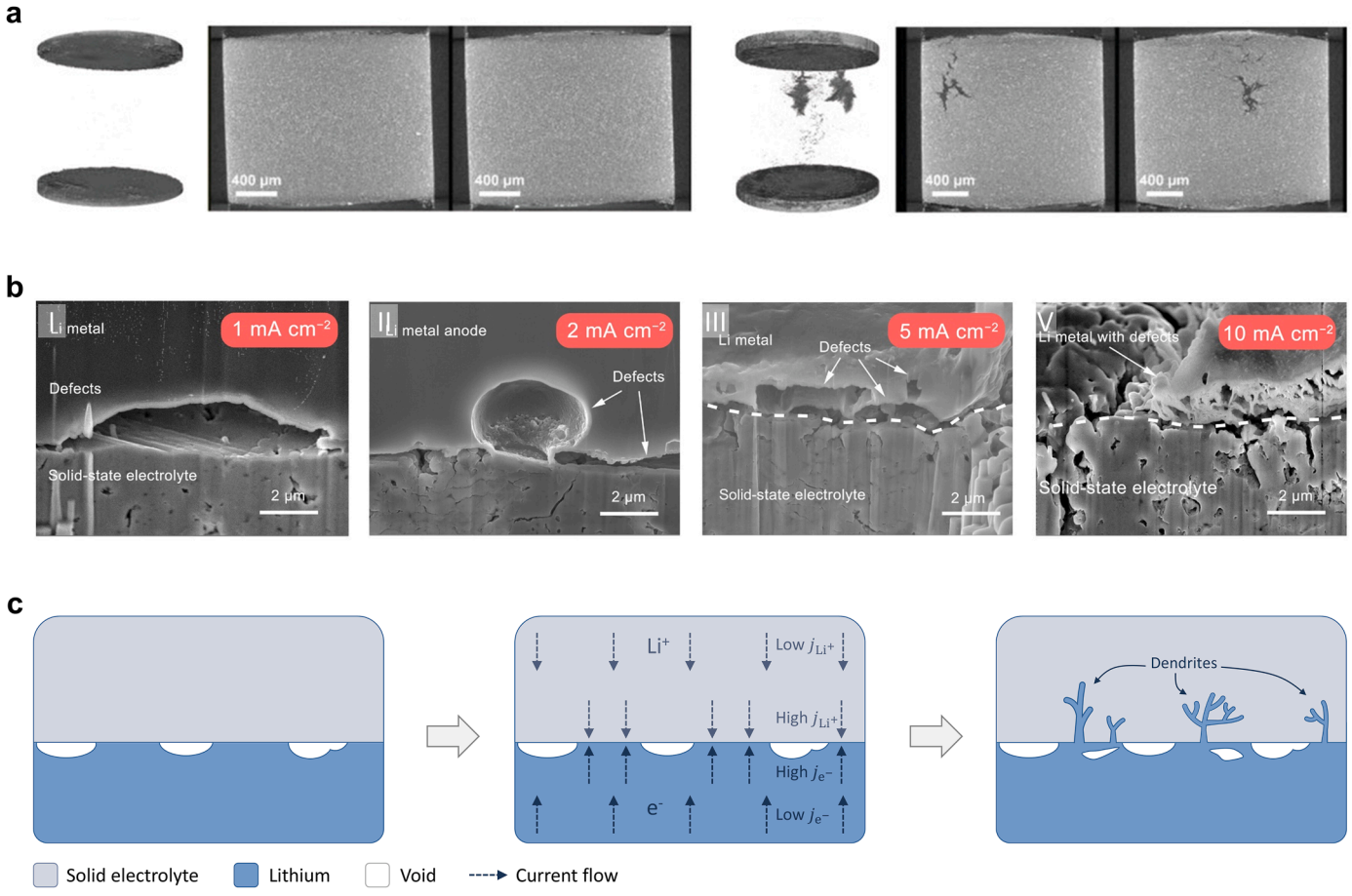

Fig. 3. Inhomogeneous interfaces, plating and stripping, and the consequences. (a) XCT scan of a symmetric cell ($Li/Li_6PS_5Cl/Li$) before plating and stripping (left) and after shorting (right), with dendrites inside the sulfide solid electrolyte [138]. (b) SEM images of the cross-section of a symmetric cell ($Li/Li_7P_3S_{11}/Li$) after 2 mAh cm^{-2} with different current densities, showing voids [153]. (c) Illustration of an inhomogeneous interface with voids between a solid electrolyte and a lithium metal anode (left). Illustration of local high current densities due to voids (center). Illustration of dendrites and voids caused by inhomogeneous plating and stripping (right).

stripping mechanisms emphasized earlier. It was discovered that higher external pressure favors a higher stripping CCD but decreases the plating CCD, which is in accordance with the enhanced creep mechanism at increased pressure [152]. Moreover, the CCD is generally higher for plating than for stripping. While in a Li/Li_6PS_5Cl/Li cell, the CCD for plating is constant against pressure variations, stripping is ten times lower at 3 MPa but only two times lower at 7 MPa when compared to the plating current density [103]. Another reason for the generally lower CCD for stripping is the connection to the additional necessary mechanisms (lithium creep and diffusion in the lithium metal) for fast stripping to maintain uniform contact. As in the case of critical plating, the more meaningful quantity is the areal capacity rather than the CCD for stripping. Especially for lithium self-diffusion and creeping, it is more difficult for lithium atoms to diffuse or creep to the interface (to maintain contact) during plating and stripping with a large areal capacity than during high current pulses involving a relatively small areal capacity (where lithium moves across the interface) [151].

Void evolution involves formation, growth, extension, and eventually, failure. Here, the determining factors are the current density for void formation (Fig. 3b) and the areal capacity for growth. Modeling void formation using the analogy of bubble formation in liquids yields the proportionality of the contact loss rate to the square of the current density [153]. As a result, emerging or preexisting voids (Fig. 3, left) cause high local current densities (Fig. 3, center); these, in turn, result in filaments inside the solid electrolyte, or dendritic filament growth from the electrode into the solid electrolyte (Fig. 3, right). Shishvan et al. [154] showed that the commonly utilized standard Butler–Volmer kinetics are not suitable for describing the observed void formation in a lithium metal anode. Instead, they used a modified version, with the result that impurity particles at the interface can be the origin of void formation due to locally inhibited flux. The merging of smaller voids into larger ones at the sulfide solid electrolyte/lithium anode interface, resulting in high local current densities, was observed by Zhao et al. [122] via *in operando* SEM with 0.2 MPa stack pressure. Furthermore, according to Lu et al. [153], vacancies are able to diffuse from the interface into the lithium metal.

Based on the lower elastic modulus, solid polymer and hybrid solid electrolytes are generally regarded as not susceptible to void formation at the solid electrolyte/anode interface. Yet, it is known that gas evolution occurs in ASSBs, which has the potential to result in the formation of gas bubbles or voids in polymers at the interface during cycling [155,156]. Among polymers, PEO exhibits a low elastic modulus with 82.80 MPa at 25 °C [157], which is significantly lower than that of typical inorganic ones, such as LLZO with > 100 GPa [158]. For hybrid solid electrolytes with PEO, the elastic modulus is typically > 100 MPa, which increases with higher proportions of filler [157]. Despite the considerably lower elastic modulus, polymer and hybrid solid electrolytes also require external stack pressure for stable cycling under high current densities. It is assumed that the application of moderate external stack pressure is not linked to solid electrolyte fracture, due to the mechanical flexibility of polymer-type solid electrolytes [157].

9. Grain boundaries and impurities

Although being electronically insulating is one of the necessary properties of a solid electrolyte, some solid electrolytes display non-negligible electronic conductivities. Electronically conductive areas can be seen as drains for electrons, interrupting the self-regulation mechanism. As a result, electrons move into the solid electrolyte to reduce lithium ions, leading to plated lithium metal inside the solid electrolyte. Possible reasons for this electronic conductivity are defects, impurities, or decomposition products [159,160]. Plated lithium metal inside the solid electrolyte provides an enhanced pathway for electrons, accelerating further filament accumulation. Investigations using *in operando* neutron depth profiling of LLZO and Li_2S–P_2S_5 solid electrolytes suggest that for dendrite-free cycling, the electronic conductivity should be lower than 10^{-10} S cm^{-1} and 10^{-12} S cm^{-1} at room temperature for plating current densities of 1 mA cm^{-2} and 10 mA cm^{-2}, respectively [161]. Comparatively, the experimentally measured and theoretically predicted electronic conductivities of sulfide, halide, and oxide inorganic solid electrolytes are beyond the limit, with $\geq 10^{-9}$ S cm^{-1} at room temperature but highly variable [159,162,163]. The influence of electronic conductivity on the CCD was found to be proportional to external applied voltage in garnet $Li_7La_{2.75}Ca_{0.25}Zr_{1.75}Nb_{0.25}O_{12}$ [164]. One consequence of electronically conductive solid electrolytes is lithium filaments plating inside the solid electrolyte, which can be accompanied by electrolyte volume expansion and increased stress inside the battery stack, as was exemplified with $Li_{1.4}Al_{0.4}Ge_{1.6}(PO_4)_3$ [165].

Grain boundaries (Fig. 4, left) are regarded as particularly prone to being electronically conductive, due to impurities or defects. The electronic pathways inside a solid electrolyte (Fig. 4, center) lead to lithium-ion reduction mainly in the grain boundary regions (Figs. 4b–d), as visualized via TEM and SEM for LLZO-based solid electrolytes [62,91,166,167]. One proposed explanation for that is a reduced band gap at the grain boundaries, which facilitates electronic transport [91]. Moreover, bigger grains lead to increased CCD, which hinders dendrite nucleation. Therefore, the electronic conductivity at grain boundaries is of critical importance [168].Crystalline defects were suggested to cause non-negligible electronic conductivity leading to lithium plating inside Li_3PS_4 solid electrolyte, observed with *in situ* optical microscopy [169]. Besides their electronic conductivity, grain boundaries seem to promote lithium nucleation due to high local ionic resistivity and physical irregularities [170]. Atomistic simulations reveal grain boundaries to be nucleation sites for lithium dendrites, with subsequent deflection and growth along the grain boundary [171]. Impurities can also cause dendrite growth in solid polymer electrolytes; this was identified via XCT study, where a globular structure observed inside a solid polymer electrolyte led to a short circuit [172]. Plated lithium inside an electronically conductive solid electrolyte is theoretically reversible because of the possibility of ions and electrons moving through the solid electrolyte, as was shown in garnet-based solid electrolytes [173,174].

10. Interphase evolution

Besides the local current density, a smaller contact area A also increases the global interfacial resistance, according to the electrical resistance $R \sim A^{-1}$ and thus the overpotential of the cell. Generally, interfacial resistance is highly dependent on the occurring reaction between the lithium metal and the solid electrolyte, because their reaction products form a solid electrolyte/electrode interphase, as shown in Figs. 5a–d. Because of the high reduction potential of lithium, solid electrolytes undergo reductive decomposition at the initial contact between solid electrolyte and lithium into electrochemically stable compounds [175].

Depending on the conduction behavior of the interphase, four different interphase growth scenarios can be expected at the solid electrolyte/lithium interface: high electronic and ionic conductive phase, low electronic and ionic conductive phase (or insulating), low electronic but high ionic conductive phase and high electronic but low ionic conductive phase [176]. With an electronic insulating interphase, the lithium anode cannot reduce the solid electrolyte further. For instance, Li_2O is found to emerge at the interface of most inorganic oxides when in contact with lithium, while Li_2S occurs at most inorganic sulfides/lithium interfaces [97,175]. Lithium oxide exhibits predominantly ionic conductivity with a low electronic conductivity [177]. In this case, lithium is plated between the Li_2O layer and the lithium anode, and the further growth of the interphase is stopped. As it has lower ionic conductivity compared to the solid electrolyte, the interphase, acting as a highly resistive layer, can limit the overall performance of the battery. Even when this is not the case, during continuous cycling, the interphase may reform and accumulate, increasing the cell resistance gradually.

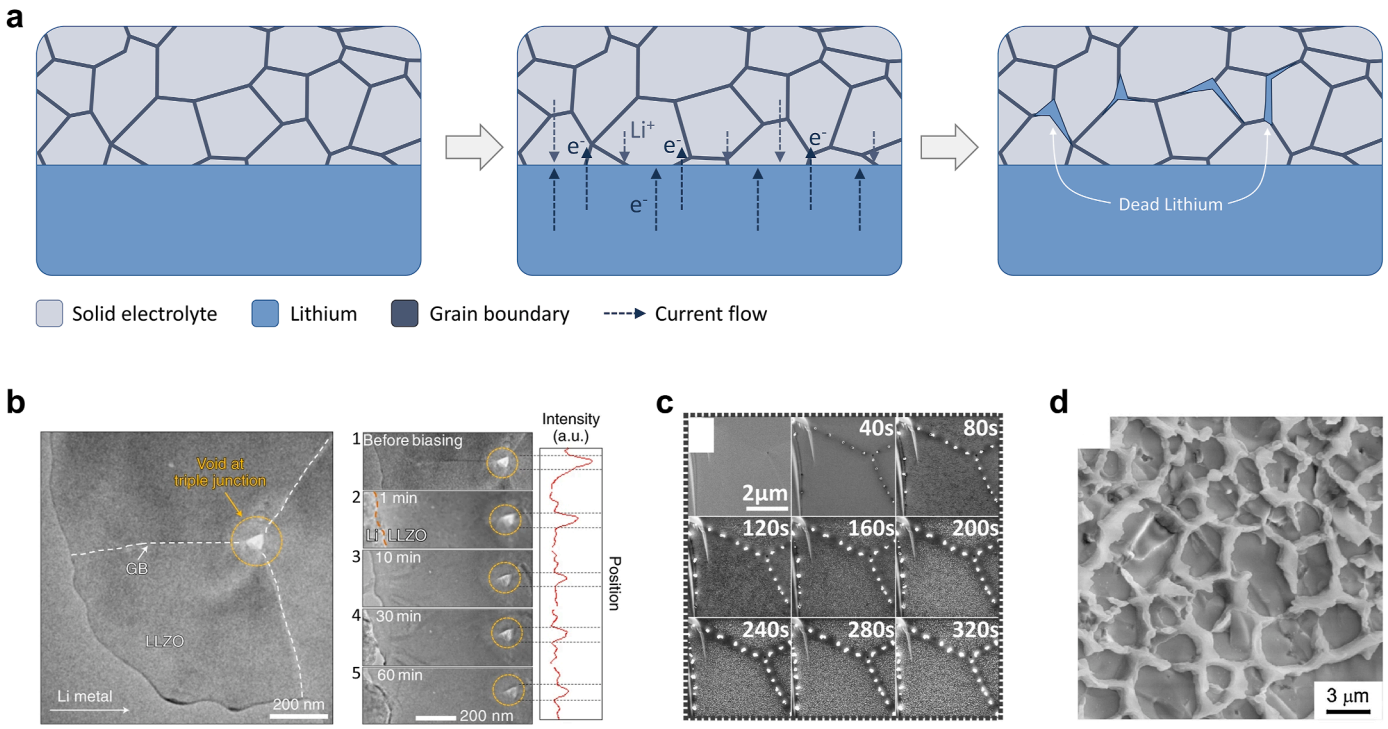

Fig. 4. Lithium metal deposition inside solid electrolytes. (a) Illustration of a solid electrolyte with grain boundaries in contact with a lithium metal anode (left). Illustration of inhomogeneous currents because of local lower ionic conductivity and electronic conductivity at the grain boundaries (center). Illustration of deposited lithium metal inside the solid electrolyte, located at the grain boundaries as a consequence of inhomogeneous plating and local electronic conductivity (right). (b) TEM image of an *in situ* formed symmetric cell ($Li/Li_7La_3Zr_2O_{12}/Cu$) in the pristine state (left and right 1) and after different times (1, 10, 30, and 60 min) with an applied potential of 10 V. The intensity course shows the corresponding intensity at the void, which is located at the triple junction [91]. (c) SEM image of a $Li_7La_3Zr_2O_{12}$ surface after different durations of electron beam irradiation, revealing grain boundaries as key locations for lithium nucleation and growth [167]. (d) SEM images of $Li_{6.25}Al_{0.25}La_3Zr_2O_{12}$ after cycling in a symmetric cell with lithium [62].

The interphase formation could be observed in the sulfide $Li_{10}SnP_2S_{12}$ electrolyte by XCT [178,179] (Figs. 5e and f) and in a solid polymer electrolyte by SEM [180] (Fig. 5g).

The solid electrolyte can be reduced by the anode, but at the same time, it can also be oxidized by the cathode [181]. This leads to the occurrence of an electrochemical window for a solid electrolyte (Fig. 6a). While aiming for minimal overpotential, the interphase can introduce local electrochemical potentials, extending the solid electrolyte's electrochemical window and stabilizing it at higher voltages (Fig. 6b). Another advantage of an interphase, if it is electronically insulating, is that it can act as a blocking mechanism for electrons entering the solid electrolyte, preventing them from forming lithium filaments once inside [182]. On the other hand, however, the emerging interphase consumes active materials in the form of lithium, lowering the Coulombic efficiency of cycling [181].

The oxidation potential of LLZO vs. Li/Li^+ was calculated to be ~3 V vs. Li/Li^+ [175], but it was experimentally determined to be 4.1–4.3 V vs. Li/Li^+ [183], which could be attributed to a protection layer formed *in situ*. However, Beabed et al. [184] reported a significantly narrower electrochemical window of 1.67–3.7 V vs. Li/Li^+ for Al-, Ta-, and Nb-substituted LLZO. The measurement was conducted with the potentiostatic intermittent titration technique on gold-supplemented LLZO to maximize the redox currents. In the case of cathodes with a regular specific capacity (e.g., NMC), a wide electrochemical window of > 4 V vs. Li/Li^+ needs to be achieved to operate an electrochemically stable battery with a desirable energy density [39]. Usually, oxide-class solid electrolytes possess a wider electrochemical window than sulfide-class ones [175]. In general, a narrow intrinsic electrochemical window for the latter is regarded as a shortcoming [185]. However, the electrochemical window is another limiting factor for fast charging combined with high capacity. Applying a higher voltage leads to an increased probability of side products, which can further increase the internal resistance and eventually lead to the loss of active material. Moreover, if the interphase density is lower than the density of the reactants, the pressure builds up or the porosity decreases as the cell compensates for the change in volume. The latter was proven with the use of XCT for a Li_3PS_4 electrolyte decomposing into the less dense components Li_2S and Li_3P [186]. In general, an even interphase layer is crucial for avoiding high local pressure or local void formation and maintaining homogeneous lithium plating and stripping [165,187].

PEO with ion-conducting salt is an example of a polymer solid electrolyte that can be cycled with an oxidation potential of 3.7–3.9 V vs. Li/Li^+, but various publications report a drastically increased electrochemical window of > 5 V vs. Li/Li^+ in combination with inorganic fillers such as LLZO [39]. Nevertheless, theoretical calculations show that the use of ion-conducting salts in polymers decreases the electrochemical window significantly (Fig. 6c) [188]. In contrast to direct decomposition by contact, an indirect decomposition pathway via lithiation (reduction) and delithiation (oxidation) of the solid electrolyte—as a kind of metastable precursor state—has been suggested for the argyrodite Li_6PS_5Cl [189]. If defined as the oxidation and reduction potential of the lithiated and delithiated solid electrolyte, the intrinsic electrochemical window for most oxides, sulfides, and halides is wider than the calculated decomposition window, based on the stability of the decomposition products (Fig. 6d) [190].

Since the interphase is a consequence of reactions between lithium and the solid electrolyte, dendrite formation will further increase interphase formation within the solid electrolyte [191]. Due to the dendrites' larger surface area, more lithium can react with the solid electrolyte, resulting in more (potentially irreversible) lithium loss. In addition to interphases playing a role in reactions at the interface with lithium, the solid electrolyte itself can feature undesirable interphases.

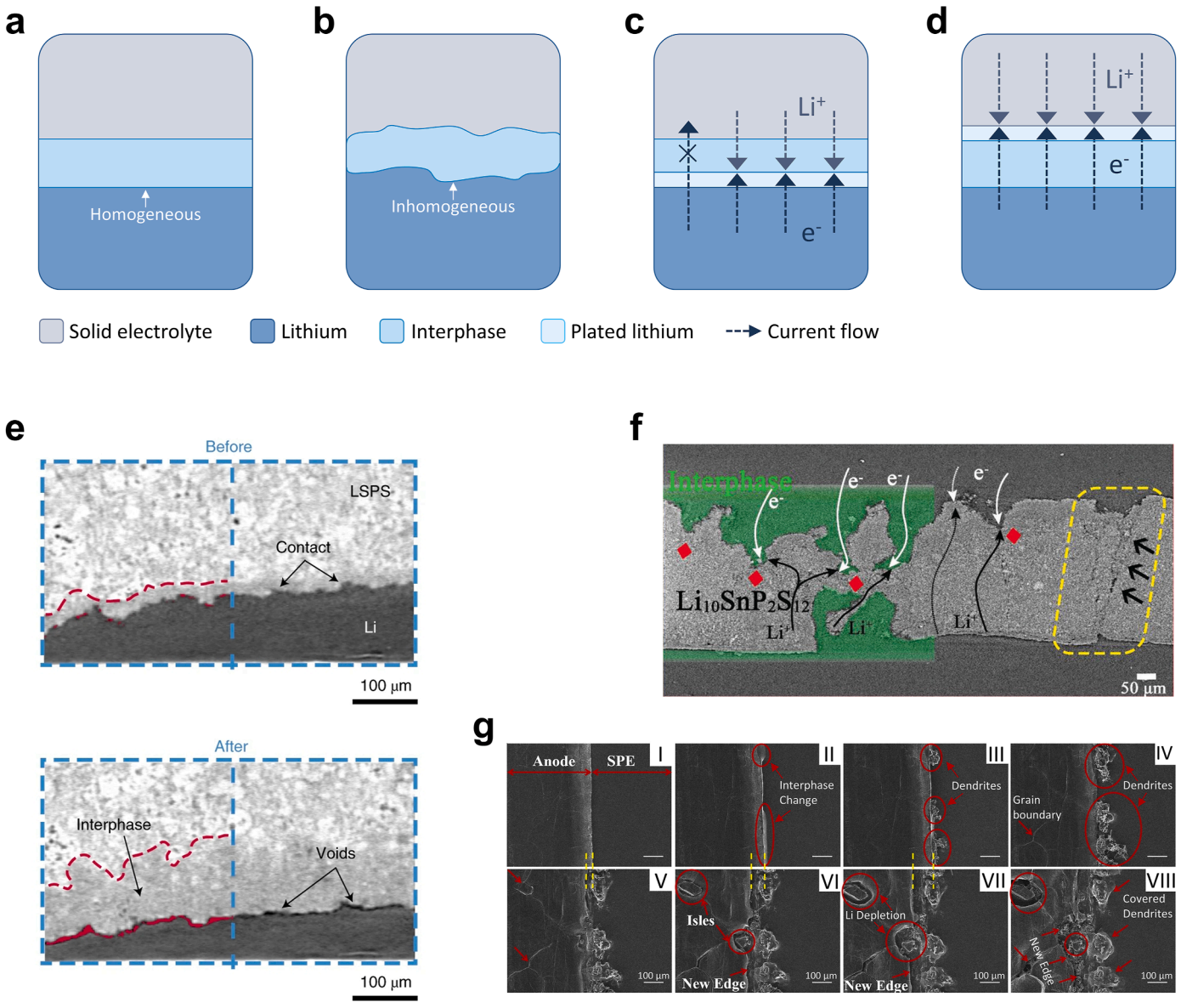

Fig. 5. Interphases between solid electrolytes and lithium metal anodes. Illustration of a homogeneous (a), inhomogeneous (b), electronic insulating, (c) and electronic conductive (d) interphase. (e) XCT images of the interphase between a solid electrolyte and a lithium anode before (top) and after (bottom) one full cycle at 1 mA cm^{-2} inside a symmetric cell ($Li/Li_{10}SnP_2S_{12}/Li$) [178]. (f) XCT scan of a symmetric cell ($Li/LiAl/Li_{10}SnP_2S_{12}/LiAl/Li$) after cycling, revealing interphase formation [179]. (g) SEM images of a solid polymer lithium anode interface: pristine (I), after 13 h (II), 14.5 h (III), 3 d (IV), 5 d (V), 7 d (VI), 8 d (VII) and 14 d (VIII) of being cycled in a full cell ($LiFePO_4$-polymer-LiTFSI/polymer-LiTFSI/Li) [180].

For example, Li_2CO_3 is found at the surface of LLZO and is regarded as a key factor in bad interfacial contact [192]. This interphase, however, emerges not due to decomposition but because of lithium-proton exchange with moisture and the subsequent reaction with CO_2 when exposed to the ambient atmosphere. Here, Li_2CO_3 is a lithium-ion blocking layer, hindering uniform ionic transport through the solid electrolyte to the anode. This effect was also reported for hybrid solid electrolytes, preventing the formation of an interphase between the PEO polymer matrix and the inorganic LLZTO filler [193].

11. Pores and cracks

Cracks either are preexisting or arise due to mechanical stress inside the solid electrolyte or at the solid electrolyte/electrode interface (Figs. 7a–d). Numerous publications suggest cracks as preferential nucleation sites for dendrites and lithium intrusion into solid electrolytes such as LLZO and LPS [121,194,195]. Cracks indicate material-free volume due to mechanical fracture or rupture. Like cracks, pores are also prone to act as nucleation sites, as has been reported for $LiBH_4$ solid electrolytes [196]. If a solid electrolyte contains a crack, the solid electrolyte must possess certain electronic conductivity for dendrite nucleation. Because of the free volume, no energy is needed to create free space for nucleation, which makes cracks or pores favorable for nucleation and subsequent dendrite growth. Moving in the crack direction without any mechanical obstacles is a low-energy pathway.

Lithium filament propagation inside a crack can enlarge the crack; however, this requires additional energy to build up the pressure needed to further crack the material. Visualized with XCT by Hao et al. [197] for Li_3PS_4 (Fig. 7e), as well by Ning et al. [198] for Li_6PS_5Cl, the tips of the cracks themselves propagate ahead of the dendrites inside them. Beyond that, cracks can cause an inhomogeneous electric field across the battery cell, which leads to dendrite propagation along the grain boundaries, as observed in LLZO [194]. Accordingly, lithium filaments can either propagate through pores or by (further) fracturing the solid electrolyte,

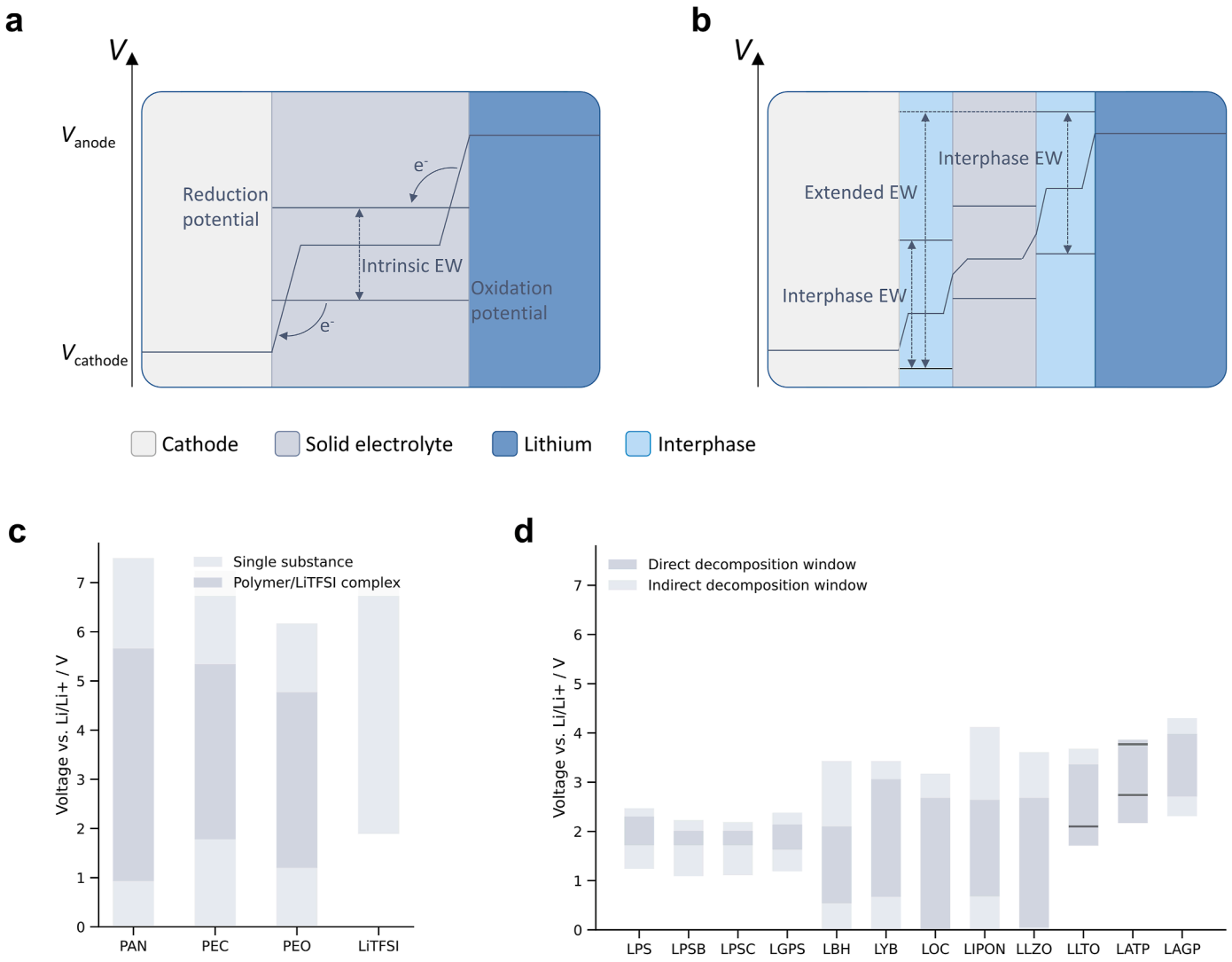

Fig. 6. Electrochemical windows of solid electrolytes. (a) Illustration of an intrinsic electrochemical window. (b) Illustration of an extended electrochemical window due to interphase (IP) formation. (c) Theoretical predicted chemical windows of different solid polymers, LiTFSI, and polymer/LiTFSI complexes (adapted from Ref. [188]). (d) Theoretically predicted direct and indirect decomposition windows for different inorganic solid electrolytes (adapted from Ref. [190]).

depending on the current density and possible structural deformation pathways [135]. In addition to serving as nucleation sites, cracks and pores can also influence the current distribution, causing non-uniform lithium deposition [199,200]. For example, it was found via XCT that argyrodite-type solid electrolytes with large particles have a better chance of building up bigger pores during pellet formation, which favors dendrite growth, compared to smaller ones that are connected with smaller pore sizes [201]. However, this is in contrast to a report that an increase in grain size favors an increase in the CCD [168]. In another study of $Li_{10}GeP_2S_{12}$ using XCT, reducing pores via applied pressure is correlated with increased ionic conductivity; this, in turn, emphasizes pores and thus, tortuosity in the diffusion path as factors influencing ionic conductivity [202]. Similarly, Melvin et al. [125] reported an increase in CCD due to the densification of lithium phosphorus sulfur chloride (LPSCl) to 99 vol%, resulting in smaller pores, as proven by FIB-SEM and XCT. It was also found that a greater distance between pores reduces the CCD.

For visualizing cracks, voids, or pores, computed tomography is heavily used in many sulfide-class solid electrolytes [101,179,195,197,198,203–209], as well as other inorganic types of solid electrolytes, such as lithium aluminum germanium phosphate (LAGP) [187] and LLZTO [210]. Although a crack-like structure in inorganic solids can be easily identified by XCT, distinguishing between an empty space and cracks filled with lithium metal is difficult due to the earlier mentioned low interactivity between lithium atoms and X-rays [211].

12. Mechanical stress

One of the most discussed dendrite formation mechanisms is propagation by fracturing due to preexisting mechanical defects in inorganic solid electrolytes. The elastic behavior of solid electrolytes is often characterized by the Young's and shear moduli. The Young's modulus describes the susceptibility to deformation under applied compressive or tensile stress [212]. The higher the Young's modulus, the smaller the deformation. Similarly, a higher shear modulus leads to less deformation compared to a lower shear modulus under an applied shear stress. If the solid was distorted in an elastic range, it will regain its initial form. But the deformation is permanent if it reaches plastic behavior. The yield strength is characterized as the smallest stress at which a solid reaches permanent deformation. From this point, a solid will experience irreversible deformation or fracture.

Another important quantity is a material's endurance of deformation—namely, the compressive strength that determines the stress that will lead to mechanical failure or irreversible deformation [212]. When

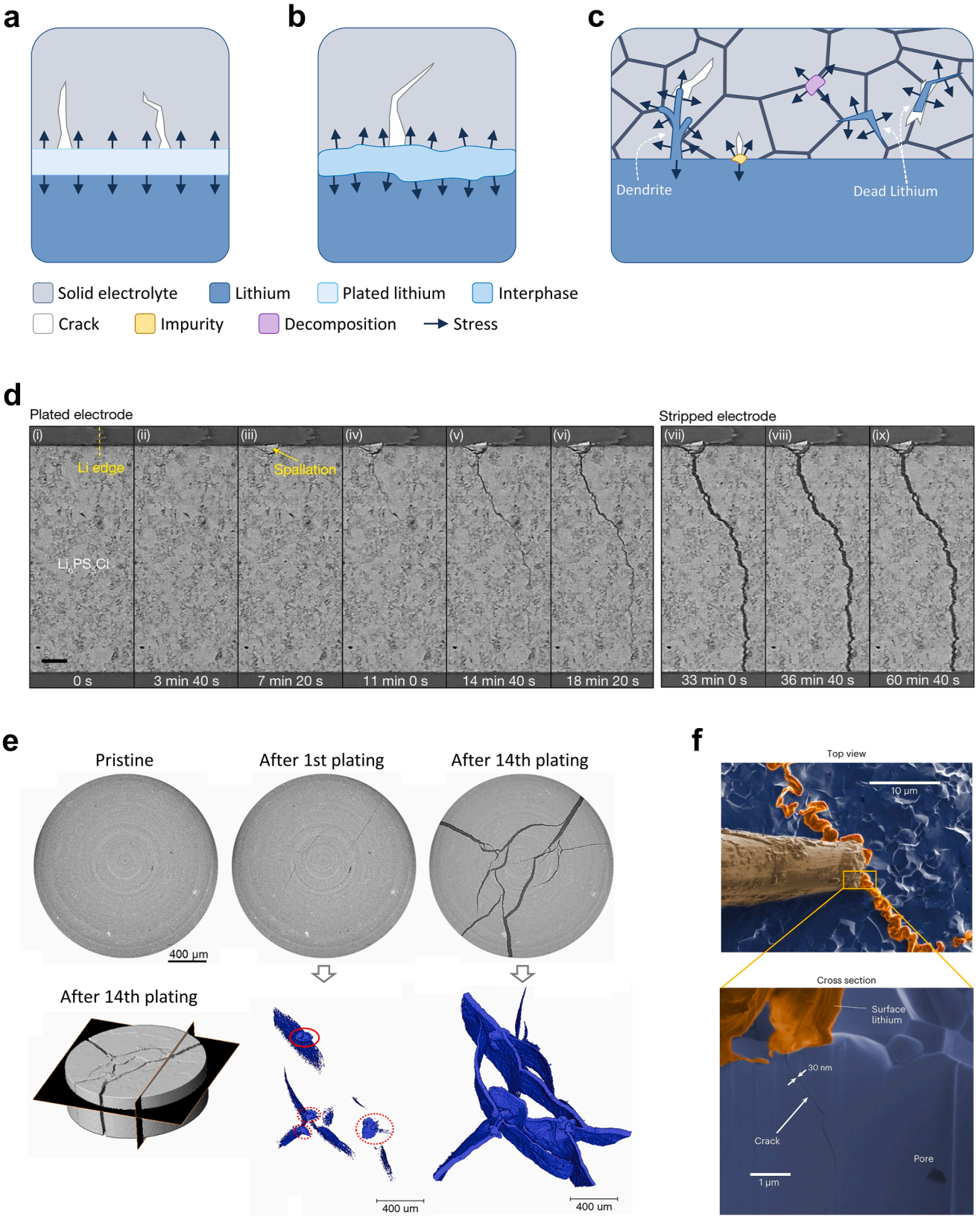

Fig. 7. Mechanical stress, followed by fracture, inside solid electrolytes. (a) Illustration of mechanical stress due to lithium plating. (b) Illustration of mechanical stress due to inhomogeneous interphase formation. (c) Illustration of local mechanical stress due to lithium dendrite growth, decomposition (purple), and impurities (yellow). (d) XCT scans of crack evolution during the cycling of a symmetric cell ($Li/Li_6PS_5Cl/Li$) with applied stack pressure [205]. (e) XCT scans of crack formation inside a solid electrolyte after symmetric cell ($Li/Li_3PS_4/Li$) cycling [197]. (f) SEM images of crack formation inside $Li_{6.6}La_3Ta_{0.4}Zr_{1.6}O_{12}$ after focused electrochemical measurements [121].

a material possesses a rupture, the fracture toughness describes the point at which further cracking becomes unrestricted. A higher fracture toughness indicates that a higher stress is needed to achieve a larger crack. Even if a material does not reach failure after a certain loading, cyclic loading can lead to failure. This is the fatigue strength, defined as the highest stress the material can withstand for a given number of cycles. Recently, Wang et al. [123] reported that lithium metal fatigue is a decisive process for understanding SSLB failure. With anisotropic materials, the point at which the stress is applied is decisive. The importance of common features like anisotropy and mechanical softness for solid electrolytes, and their significance for blocking lithium dendrite formation, were emphasized by Ahmad et al. [213]. They theoretically found four solid electrolytes that are soft, highly anisotropic, and ionically conductive and that could build a dendrite-suppressing interface with lithium.

Calculations show that lithium can grow at the lithium/solid interface if the interfacial transfer resistance is greater than approximately 14 $\Omega\,cm^2$ [170].This is in agreement with Porz et al. [214], who reported that the interfacial overpotential for crack propagation at flaws is rather low, especially for micro-size defects. Consequently, higher overpotential correlates with amplified crack propagation. Modeling of electrodeposition revealed that as soon as the pressure from lithium plating at the crack tip exceeds the fracture toughness of an inorganic solid electrolyte, the crack propagates rapidly [199]. The fracture toughness of LLZO is in the order of 1 MPa $m^{0.5}$, whereby the magnitude is dependent on the grain size [215]. Since increased grain size is associated with a higher elastic modulus and higher hardness, mechanical load when investigating the effect of grain size on dendrites must also be taken into account alongside the electronic properties. On the other hand, because the stress related to dendrite growth is about 1 kPa but the fracture stress of LLZO is in the MPa range, the factorial penetration of lithium dendrites through LLZO suggests an additional mechanism is involved in dendrite propagation other than just the mechanical ones [216]. This can be explained by the fact that insufficient lithium atom diffusion causes a decrease in contact area, which, in turn, increases the local pressure significantly past the fracture stress of LLZO. Based on the chemical potential change, it was calculated that the balancing back-stress for opposing lithium dendrite nucleation equals the effective fracture stress of the solid electrolyte (e.g., 100 MPa for ceramics) [170]. The same goes for the earlier conditions proposed by Monroe and Newman [217,218] for solid polymers using mechanically enhanced systems, such that one should be designed with a high shear modulus to avoid dendrite growth. This was later found not to be the determining factor for dendrite prevention and thus not a sufficient criterion, even in inorganic solids [214]. Nevertheless, a larger fracture toughness is regarded as mechanism for combating dendrite growth, because it suppresses crack propagation [219]. Interestingly, in addition to that, it was also found that an increased Young's modulus can either favor or stop cracking, depending on the magnitude, although a direct correlation is probably lacking [219].

As well as preexisting cracks, localized lithium plating can be followed by localized pressure distribution, which, in turn, can cause cracking with further stress [220]. Conversely, local stress variation influences both the diffusion coefficient of the conductive ions and the interfacial charge transfer resistance through deformation-induced energy changes, crack generation, and interface modification [221–223]. Generally, mechanical stress has a minimal effect on ion diffusion within the lattice when local stress is in the MPa range [223,224], but if the stress is in the GPa range, the ion diffusion within the lattice is reduced and the activation energy increases [223,225–228]. Similarly, interfacial contact resistance can be improved with stress by improving the contact, but excessive stress will cause fragmentation of the material, leading to increased contact resistance. Also, when pores are filled by deposited lithium, enough pressure can develop to crack the solid electrolyte. Low hardness (resistance to local plastic deformation) is beneficial for avoiding cracking under pressure, but it is also a disadvantage for impeding dendrite propagation, because less energy is needed to penetrate the material. Thus, lithium filaments can penetrate solid polymer electrolytes easily once they are formed. In the case of solid polymer electrolytes, despite their soft nature, pressure still matters. Recently, it was reported that insufficient pressure can lead to void formation, while excessive pressure can mechanically damage a solid polymer electrolyte [229]. Adding inorganic fillers increases the CCD by introducing an obstacle for dendrites and enhancing the mechanical strength [230,231]. As the filler proportion increases, so does the mechanical strength of the hybrid solid electrolyte [232]. However, for a hybrid solid electrolyte, it was shown via *in operando* XCT that when the electrolyte was compressed with a low pressure of 0.7 MPa, movement of individual inorganic fillers resulted, potentially lowering the mechanical strength [116]. How lithium metal dendrites interact with an inorganic filler can differ, depending on the filler material. While LAGP fillers chemically interact with dendrites, LLZO fillers primarily form a physical barrier, as revealed by a combination of solid-state NMR spectroscopy and Overhauser dynamic nuclear polarization [233].

Flaws, like cracks, propagate not only due to further filling with lithium filaments but also through local stresses caused by uneven, volumetric growth of the interphase and reaction products, and lithium plating at the anode or inside the solid electrolyte. Regular plating leads to pressure build-up; this, in turn, causes mechanical deformation, as was found by *in situ* curvature measurements of a LLZO electrolyte [234]. During a short-circuit event, a pressure change in the lithium metal was measured, indicating a fracture incident in the solid electrolyte. In general, it is assumed that rapid crack propagation can also be triggered by externally applied stacking pressure [149,235]. This would suggest that safe operation requires either a higher fracture strain for rigid, mostly inorganic, solid electrolytes to avoid crack propagation, or less external pressure. Organic polymers, by contrast, are resistant against fracture under pressure to some degree, due to the low elastic modulus previously mentioned. Instead of cracking, they more easily undergo deformation to balance the pressure. Similarly, lithium with a Young's modulus and a shear modulus of 7.82 and 2.83 GPa, respectively, undergoes deformation instead of fracture under high pressure [104]. Another important factor is the distribution of the exerted force, which can result in local high pressure even when the global pressure is low. For example, contaminating particles at the interface can act as additional local pressure sources in inorganic solid electrolytes such as LLZO [121]. Depending on their mechanical properties, they can act as “center punches” when pressure builds up, promoting fractures. Beyond the electrolyte, it needs to be considered that the cathode can also undergo fracture due to pressure changes resulting from lithiation and delithiation, such as the cracking of NMC particles observed with XCT [236,237]. This ought to be taken into account in the search for an optimal pressure, in line with moderate mechanical stress in every battery component.

Comparatively, solid-state polymer electrolytes offer the unique ability to circumvent these mechanical challenges when designed to exhibit viscoelastic properties through synthetically engineered backbones, topologies, and crosslinking dynamism. For example, a dynamic polymer network allows mechanical dissipation through a combination of backbone creep and reversible crosslinking bond exchange, enabling it to repair microcracks, reorganize poor-contact interfaces that would otherwise concentrate the current, and trigger localized deposition [50, 238,239].

Besides mechanically induced stress, electrochemically derived stress due to high local currents is also able to fracture a solid electrolyte, as has been shown by TEM [240] and SEM [121] (Fig. 7f) for LLZO. Similarly, modelling reveals that voids lead to a nonuniform lithium-ion distribution inside an inorganic solid electrolyte close to the void edge, ultimately causing mechanical stress and possibly leading to cracks [149].

Above all, the difference between internal and external pressure in relation to possible local stress-generation sources must be considered [241].

13. Dendrite growth and its consequences

Among all of the degradation processes and inhomogeneities—such as decomposition products inside the solid electrolyte, voids, pores, and cracks (Fig. 8a)—undesirable lithium filaments, in particular, can lead to severe consequences. In the worst case, dendrites build an electronic conductive bridge between the anode and the cathode, resulting in a short circuit that unloads all the stored energy at once (hard short circuit, Fig. 8b). But when the dendrites are narrow enough, total cell failure may be averted in all-solid-state batteries due to the low melting point of lithium (soft short circuit). Dendrite tips are prone to accumulate currents due to their low-resistance pathway for electrons and high electrochemical overpotential for ions. This high current can lead to heat dissipation and a high enough temperature to melt lithium, causing some dendrites to disconnect from the network [220,242]. The process is often described as a dendrite self-healing mechanism, as cell operation is in most cases still possible after such an event in all-solid-state batteries. Nevertheless, it affects the cell, and multiple thin dendrites may coalesce to form a hard short circuit [242]. Beside lithium dendrites, the electronic conductivity of solid electrolytes entails an electronic bridge that can lead to self-discharge, which lowers the stored energy in the charged state (Fig. 8c) [243].

Furthermore, dendrites, if not reversible, can cause the loss of lithium inventory. The formation of "dead lithium" is characterized by the occurrence of lithium metal, often in dendritic form, becoming disconnected from the anode active materials during cycling. Hence, further stripping of the lithium via the anode becomes impossible (Fig. 8d) [244]. This occurs due to either an electronic insulating solid

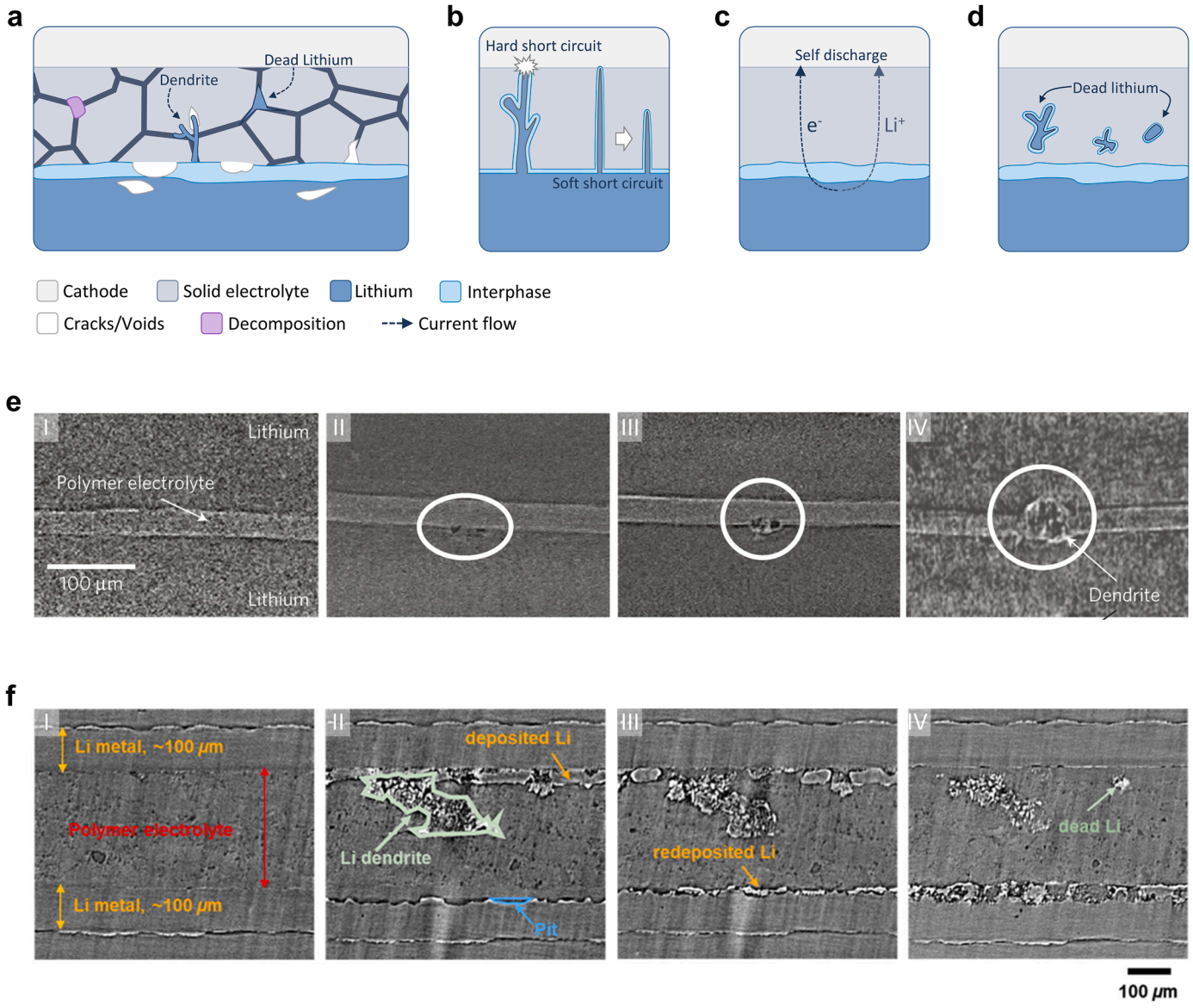

Fig. 8. Cell consequences of degradation mechanisms. (a) Illustration of decomposition (purple), dendrites, lithium filaments, and cracks inside the solid electrolyte, with voids inside the lithium anode and interphase formation, which causes an increased overpotential. (b) Illustration of a hard short circuit (left) and a soft short circuit (right). (c) Illustration of self-discharge due to electronic conductivity of the solid electrolyte. (d) Illustration of dead lithium with interphase inside the solid electrolyte. (e) XCT scan of a symmetric cell (Li/solid polymer/Li) in the pristine state (I), after 9 C cm^{-2} (II), 84 C cm^{-2} (III), and shorted after 296 C cm^{-2} (IV), with dendritic structures [250]. (f) XCT scans showing the evolution of degradation mechanisms inside a symmetric cell (Li/polymer/Li) in the pristine state (I), during charging (II), during discharging (III), and after 1 full cycle (IV) [257].

electrolyte or a lithium-ion or electron-blocking interphase forming around the filaments.

How dendrites penetrate a solid electrolyte depends on several parameters. The dendrite growth direction seems to be pressure dependent, since dendrites can be deflected in a LLZTO electrolyte with an in-plane applied stress, regardless of the initial orientation [245]. Not only the growth rate but also the morphology of dendrites is dependent on the current density [246] and the solid electrolyte type [247]. According to the classification by Kazyak et al. [248], there are four different types of lithium filament growth through ceramic solid electrolytes: straight, branching, spalling, and diffusive. While mossy, needle, and bump-like dendrite morphologies were observed via SEM on a lithium surface using LLZO as the solid electrolyte [249], dendrites in solid polymer electrolytes were reported to evolve in a globule-like structure, as revealed via XCT (Fig. 8e) [250]. For single-crystal LLZTO, it was found via darkfield X-ray microscopy that dislocations appear in the proximity of dendrite tips, which suggests that dendrite expansion induced dislocation, eventually leading to branching dendrite growth [251]. As polymers conduct both cations and anions, a space charge layer can develop through the dissimilar transport of cations and anions in the solid electrolyte. Chazalviel suggested such an electrical field as a possible reason for dendrite growth [252]. Based on Chazalviel's model, it has been proposed that the time before a dendrite in a polymer short-circuits the cell is composed of the dendrite growth onset time (commonly called Sand's time) and the growth time from the anode to the cathode [253]. Knowing those times can aid in understanding dendrite growth and how to improve dendrite resistance by tuning the relevant parameters [254].

A theoretical comparison between lithium filament nucleation at the solid electrolyte/anode interface and at grain boundaries reveals that the critical current density is approximately two orders of magnitude higher at the grain boundaries. This suggests that the interface is a favorable nucleation site in inorganic solids, although the higher dendrite initiation resistance could be at the interface [182]. In contrast, it was reported that when the stress at the interface is high enough and it is energetically favored, lithium forms a new phase between grains of LLZO in a grain-coating-like process [255]. This, in turn, suggests that the dendrite nucleation and propagation processes do not necessarily require mechanical fracture in inorganic solid electrolytes. For hybrid solid electrolytes, the cell resistance against dendrite growth can be influenced by the ceramic loading, based on the coupling of increased stiffness with increased filler share [70,256].

Many of the addressed mechanisms, such as interphase or void formation, contribute to a higher overpotential. Overall, these events lower the battery performance due to lower possible stripping and plating current, and the overall useable energy inside the battery cell. Since some of these processes are a consequence of just a single or several cycling periods, they continuously lower the Coulombic efficiency. In most cases, several processes take place simultaneously. For example, the dendrite formation in a solid polymer electrolyte can be accompanied by various degradation mechanisms at the same time, like void and dead lithium formation, as has been shown via XCT (Fig. 8f) [257].

14. Summary and outlook

SSLBs have the potential to be next-generation high-energy-density batteries. Unfortunately, different degradation mechanisms, in particular dendrite formation, are limiting their performance and lifetime. Moreover, even if the factors hindering performance are eliminated, the material and processing costs for solid electrolytes must also be decreased for these batteries to become commercially attractive [258,259]. Understanding the processes behind the different degradation and conduction mechanisms is the major key to achieving the commercialization of SSLBs. For this purpose, microscopic characterization appears to bring the most valuable insights.

While the ionic conductivities of sulfide and oxide solid electrolytes are already at a promising order of magnitude, the polymer solid electrolytes thus far reported have not reached those scales. Adding inorganic filler to polymer systems can enhance the ionic conductivity significantly, but lithium ions seem not to hop between systems consisting of organic and inorganic phases, such as LLZO/PEO. This, in turn, means limiting the filler share due to the consequent increase in tortuosity. Furthermore, to achieve sufficient segmental motion, solid polymer electrolytes need to be cycled at elevated temperatures, which decreases the energy efficiency and limits the possible applications of solid electrolytes [1]. Therefore, developing polymer and hybrid solid electrolyte systems that can operate at ambient temperatures would increase the potential for commercial use.

Grain boundaries in inorganic solid electrolytes are one of the most crucial microscopic properties and thus are intertwined with ionic conductivity, electronic conductivity, and undesired lithium filament growth. Therefore, controlling the grain boundary size or chemical composition is important, but also challenging. For example, while fewer grain boundaries, and thus bigger grains, are reported to correlate with lower electronic conductivity and fewer nucleation sites, they are also correlated with more pores, and thus, dendrite nucleation sites. The same conflict applies when it comes to pressure. While pressure in general is needed to provide adequate contact in a solid electrolyte/electrode interface, exceeding a certain threshold can lead to microcracks and lithium creep inside the solid electrolyte [260]. Beyond that, the technical side needs to be considered: an operational pressure below 0.1 MPa (i.e., 1 atm) is ideal, but a few MPa are still regarded as practicable for all-solid-state batteries [261]. Consequently, the development of battery cells capable of operating at low stack pressures is a highly desirable objective.

Lithium dendrites are the most severe consequences of inhomogeneous plating and stripping and must be avoided. Understanding how and where they are nucleating and propagating remains one of the main challenges. Similarly, interphases are critical and cannot be avoided, but a comprehensive knowledge about their chemical composition and evolution is necessary to prevent destructive ones and allow those that improve performance.

In addition, unavoidable deviations always need to be considered—specifically, where an experimental model cell system can differ from commercially used cells. For example, symmetric cells, which are commonly used to investigate solid electrolyte performance, differ from full cells and can overestimate the growth of dendrites through a solid electrolyte [262].

The interconnectedness of diverse degradation mechanisms (Fig. 2c) emphasizes the difficulties involved and the importance of disentangling these processes to tackle each issue precisely. This review has stressed the importance of avoiding impurities, cracks, pores, or other chemical and mechanical flaws inside the solid electrolyte and at the solid electrolyte/electrode interface. When an SSLB is operating at ambient pressure, it is crucial to overcome the low self-diffusion of lithium to suppress void formation at the solid electrolyte/lithium anode interface. One solution is modifying the lithium metal anode by substituting other elements such as indium (widely used) [263,264] or sodium (recently reported) [265], ultimately forming an alloy anode. On the other hand, operating SSLBs with high external pressure in the range of tens of MPa to avoid void formation at the solid electrolyte/lithium anode interface by promoting lithium creep is feasible at the laboratory scale. However, how the lithium creep affects the long-term cell life of SSLBs should be studied as well. Any degradation mechanism is directly or indirectly connected to inhomogeneous plating or stripping and thus to dendrite formation, capacity loss, and higher overpotential, restricting the energy and power density and lifetime, and ultimately resulting in poorer overall performance.

The lithium metal anode is the dominant side when it comes to stress due to volume expansion and contraction during charging and discharging, even at low stack pressures [266]. Nevertheless, a typical

intercalation cathode such as NMC can also cause significant mechanical stress during charging and discharging, representing a possible degradation mechanism that needs to be considered for a holistic view on the battery.

Looking ahead, identifying the microscopic origins of failures in SSLB systems will also provide insights for materials research and battery cell design aimed at stabilizing solid-state electrolyte systems by resolving these issues precisely. For example, protective electrolyte–electrode interlayers composed of gold [267], carbon, inorganic composites [268], and polymers [145,269] have demonstrated advantageous effects by modulating the interfacial transference properties, thus stabilizing SSEs against dendrite formation and other failure modes, and thereby significantly prolonging the cycle life of the SSLBs. With more comprehensive insights, materials with well-studied properties in different fields or other battery applications can be better engineered to resolve the identified issues for SSLBs as well. For example, dynamic, self-healing polymer electrolytes and composites offer unique advantages in terms of reorganization and mechanical stress dissipation, circumventing the common challenges encountered in rigid inorganic electrolytes that would otherwise require high stack pressure operation, while also supporting cell cycling by maintaining ion-selective transport and electrode–electrolyte interface stabilization [270–275].

The ability to homogenize mass transport and maintain conformable coverage can lessen the chance of failure brought about by structural inhomogeneity and volume changes during battery cycling. We anticipate that novel materials design guided by a deeper understanding of failure mechanisms will enable new opportunities for developing stable SSLBs, generating next-generation safe, reliable solutions for electrification.

CRediT authorship contribution statement

Luca Weckelmann: Writing – review & editing, Writing – original draft, Visualization, Formal analysis, Data curation, Conceptualization. **Hao Lyu:** Writing – review & editing, Supervision, Conceptualization. **Han Yang:** Writing – original draft, Data curation, Conceptualization. **Chih-Long Tsai:** Writing – review & editing, Writing – original draft, Supervision, Resources, Project administration, Funding acquisition, Conceptualization. **Krzysztof Dzieciol:** Writing – review & editing, Supervision, Conceptualization. **Shicheng Yu:** Writing – review & editing. **Anna Windmüller:** Writing – review & editing, Funding acquisition. **Hans Kungl:** Writing – review & editing, Supervision, Project administration. **Zhenan Bao:** Writing – review & editing, Supervision, Resources, Project administration, Funding acquisition. **Rüdiger-A. Eichel:** Writing – review & editing, Supervision, Project administration, Funding acquisition.

Conflict of interest

The authors declare no conflict of interest and no competing financial interest.

Acknowledgements

The authors would like to acknowledge funding support from the “US–German Cooperation on Energy Storage” project, within the “LISI-2-Lithium-Solid-Electrolyte Interfaces” funding program (project no. 13XP0509A) of the Federal Ministry for Research, Technology and Aeronautics (BMFTR) and the US Department of Energy (DOE), and from the “High Performance Solid-State Batteries” (HIPSTER) project of the Ministerium für Kultur und Wissenschaft des Landes Nordrhein-Westfalen.

References

[1] T. Schmaltz, T. Wicke, L. Weymann, P. Voß, C. Neef, A. Thielmann, Solid-state battery roadmap 2035+, 2022.
[2] X. Tang, S. Lv, K. Jiang, G. Zhou, X. Liu, Recent development of ionic liquid-based electrolytes in lithium-ion batteries, J. Power Sources 542 (2022) 231792.
[3] Z. Zhang, W.-Q. Han, From liquid to solid-state lithium metal batteries: fundamental issues and recent developments, Nano-Micro Lett. 16 (2023) 24.
[4] Y. Chen, Y. Kang, Y. Zhao, L. Wang, J. Liu, Y. Li, Z. Liang, X. He, X. Li, N. Tavajohi, B. Li, A review of lithium-ion battery safety concerns: the issues, strategies, and testing standards, J. Energy Chem. 59 (2021) 83–99.
[5] S.K. Sharma, G. Sharma, A. Gaur, A. Arya, F. Sadat Mirsafi, R. Abolhassani, H.-G. Rubahn, J.-S. Yu, Y. Kumar Mishra, Progress in electrode and electrolyte materials: path to all-solid-state Li-ion batteries, Energy Adv. 1 (2022) 457–510.
[6] S. Xia, X. Wu, Z. Zhang, Y. Cui, W. Liu, Practical challenges and future perspectives of all-solid-state lithium-metal batteries, Chem 5 (2019) 753–785.
[7] S. Kainat, J. Anwer, A. Hamid, N. Gull, S.M. Khan, Electrolytes in lithium-ion batteries: advancements in the era of twenties (2020's), Mater. Chem. Phys. 313 (2024) 128796.
[8] M. Nojabaee, D. Kopljar, N. Wagner, K.A. Friedrich, Understanding the nature of solid-electrolyte interphase on lithium metal in liquid electrolytes: a review on growth, properties, and application-related challenges, Batter. Supercaps 4 (2021) 909–922.
[9] H. Adenusi, G.A. Chass, S. Passerini, K.V. Tian, G. Chen, Lithium batteries and the solid electrolyte interphase (sei)—progress and outlook, Adv. Energy Mater. 13 (2023) 2203307.
[10] G. Brunklaus, P. Lennartz, M. Winter, Metal electrodes for next-generation rechargeable batteries, Nat. Rev. Electr. Eng. 1 (2024) 79–92.
[11] J. Betz, G. Bieker, P. Meister, T. Placke, M. Winter, R. Schmuch, Theoretical versus practical energy: a plea for more transparency in the energy calculation of different rechargeable battery systems, Adv. Energy Mater. 9 (2019) 1900761.
[12] S. Weng, G. Yang, S. Zhang, X. Liu, X. Zhang, Z. Liu, M. Cao, M.N. Ateş, Y. Li, L. Chen, Z. Wang, X. Wang, Kinetic limits of graphite anode for fast-charging lithium-ion batteries, Nano-Micro Lett. 15 (2023) 215.
[13] J. Ulrich, A. Lindner, T. Brake, M. Winter, S. Wiemers-Meyer, A. Weber, U. Krewer, Early detection of lithium plating during fast charging of lithium-ion batteries using nonlinear frequency response analysis, J. Power Sources 647 (2025) 237358.
[14] X. Ke, Y. Wang, L. Dai, C. Yuan, Cell failures of all-solid-state lithium metal batteries with inorganic solid electrolytes: lithium dendrites, Energy Storage Mater. 33 (2020) 309–328.
[15] Q. Wu, S. Xiong, F. Li, A. Matic, Electro-chemo-mechanical failure mechanisms of solid-state electrolytes, Batter. Supercaps 6 (2023) e202300321.
[16] F.-N. Jiang, S.-J. Yang, H. Liu, X.-B. Cheng, L. Liu, R. Xiang, Q. Zhang, S. Kaskel, J.-Q. Huang, Mechanism understanding for stripping electrochemistry of Li metal anode, SusMat 1 (2021) 506–536.
[17] Z. Yu, X. Zhang, C. Fu, H. Wang, M. Chen, G. Yin, H. Huo, J. Wang, Dendrites in solid-state batteries: ion transport behavior, advanced characterization, and interface regulation, Adv. Energy Mater. 11 (2021) 2003250.
[18] B. Zhang, R. Tan, L. Yang, J. Zheng, K. Zhang, S. Mo, Z. Lin, F. Pan, Mechanisms and properties of ion-transport in inorganic solid electrolytes, Energy Storage Mater. 10 (2018) 139–159.
[19] Q. Yang, A. Wang, J. Luo, W. Tang, Improving ionic conductivity of polymer-based solid electrolytes for lithium metal batteries, Chin. J. Chem. Eng. 43 (2022) 202–215.
[20] Z. Xue, D. He, X. Xie, Poly(ethylene oxide)-based electrolytes for lithium-ion batteries, J. Mater. Chem. A 3 (2015) 19218–19253.
[21] V. Raj, N.P.B. Aetukuri, J. Nanda, Solid state lithium metal batteries – issues and challenges at the lithium-solid electrolyte interface, Curr. Opin. Solid State Mater. Sci. 26 (2022) 100999.
[22] K.B. Oldham, C.G. Zoski, Chapter 2 mass transport to electrodes, Compr. Chem. Kinet. 26 (1986) 79–143.
[23] H. Yang, N. Wu, Ionic conductivity and ion transport mechanisms of solid-state lithium-ion battery electrolytes: a review, Energy Sci. Eng. 10 (2022) 1643–1671.
[24] T. Famprikis, P. Canepa, J.A. Dawson, M.S. Islam, C. Masquelier, Fundamentals of inorganic solid-state electrolytes for batteries, Nat. Mater. 18 (2019) 1278–1291.
[25] Z.-H. Fu, X. Chen, Q. Zhang, Review on the lithium transport mechanism in solid-state battery materials, WIREs Comput. Mol. Sci. 13 (2023) e1621.
[26] R.J. Friauf, Correlation effects for diffusion in ionic crystals, J. Appl. Phys. 33 (2004) 494–505.
[27] G.E. Murch, The haven ratio in fast ionic conductors, Solid State Ion 7 (1982) 177–198.
[28] G.E. Murch, Diffusion kinetics in solids, Mater. Sci. Technol. (2013).
[29] J. Kawamura, R. Asayama, N. Kuwata, O. Kamishima, Ionic transport in glass and polymer : hierarchical structure and dynamics, Physics Solid State Ion (2006) 193–246.
[30] C. Wang, B.B. Xu, X. Zhang, W. Sun, J. Chen, H. Pan, M. Yan, Y. Jiang, Ion hopping: design principles for strategies to improve ionic conductivity for inorganic solid electrolytes, Small 18 (2022) 2107064.
[31] S. Muy, R. Schlem, Y. Shao-Horn, W.G. Zeier, Phonon–ion interactions: designing ion mobility based on lattice dynamics, Adv. Energy Mater. 11 (2021) 2002787.
[32] Y. Wang, W.D. Richards, S.P. Ong, L.J. Miara, J.C. Kim, Y. Mo, G. Ceder, Design principles for solid-state lithium superionic conductors, Nat. Mater. 14 (2015) 1026–1031.
[33] M. Wu, B. Xu, C. Ouyang, Physics of electron and lithium-ion transport in electrode materials for li-ion batteries, Chin. Phys. B 25 (2015) 018206.
[34] J.G. Smith, D.J. Siegel, Low-temperature paddlewheel effect in glassy solid electrolytes, Nat. Commun. 11 (2020) 1483.
[35] Z. Zhang, H. Li, K. Kaup, L. Zhou, P.-N. Roy, L.F. Nazar, Targeting superionic conductivity by turning on anion rotation at room temperature in fast ion conductors, Matter 2 (2020) 1667–1684.

[36] Y. Sun, Y. Wang, X. Liang, Y. Xia, L. Peng, H. Jia, H. Li, L. Bai, J. Feng, H. Jiang, J. Xie, Rotational cluster anion enabling superionic conductivity in sodium-rich antiperovskite Na_3OBH_4, J. Am. Chem. Soc. 141 (2019) 5640–5644.
[37] Z. Zhang, P.-N. Roy, H. Li, M. Avdeev, L.F. Nazar, Coupled cation–anion dynamics enhances cation mobility in room-temperature superionic solid-state electrolytes, J. Am. Chem. Soc. 141 (2019) 19360–19372.
[38] Z. Zhang, L.F. Nazar, Exploiting the paddle-wheel mechanism for the design of fast ion conductors, Nat. Rev. Mater. 7 (2022) 389–405.
[39] S. Huo, L. Sheng, W. Xue, L. Wang, H. Xu, H. Zhang, X. He, Challenges of polymer electrolyte with wide electrochemical window for high energy solid-state lithium batteries, InfoMat 5 (2023) e12394.
[40] Z. Song, F. Chen, M. Martinez-Ibañez, W. Feng, M. Forsyth, Z. Zhou, M. Armand, H. Zhang, A reflection on polymer electrolytes for solid-state lithium metal batteries, Nat. Commun. 14 (2023) 4884.
[41] W.H. Meyer, Polymer electrolytes for lithium-ion batteries, Adv. Mater. 10 (1998) 439–448.
[42] Z. Li, J. Fu, X. Zhou, S. Gui, L. Wei, H. Yang, H. Li, X. Guo, Ionic conduction in polymer-based solid electrolytes, Adv. Sci. 10 (2023) 2201718.
[43] Z. Gadjourova, Y.G. Andreev, D.P. Tunstall, P.G. Bruce, Ionic conductivity in crystalline polymer electrolytes, Nature 412 (2001) 520–523.
[44] V. St-Onge, M. Cui, S. Rochon, J.-C. Daigle, J.P. Claverie, Reducing crystallinity in solid polymer electrolytes for lithium-metal batteries via statistical copolymerization, Commun. Mater. 2 (2021) 83.
[45] C.-W. Chang, W.-C. Lai, A strategy for preparing solid polymer electrolytes via the electrospinning process, J. Taiwan Inst. Chem. Eng. 116 (2020) 279–285.
[46] N.S. Schauser, A. Nikolaev, P.M. Richardson, S. Xie, K. Johnson, E.M. Susca, H. Wang, R. Seshadri, R.J. Clément, J. Read de Alaniz, R.A. Segalman, Glass transition temperature and ion binding determine conductivity and lithium–ion transport in polymer electrolytes, ACS Macro Lett. 10 (2021) 104–109.
[47] F. Müller-Plathe, W.F. van Gunsteren, Computer simulation of a polymer electrolyte: lithium iodide in amorphous poly(ethylene oxide), J. Chem. Phys. 103 (1995) 4745–4756.
[48] A. Marinow, Z. Katcharava, W.H. Binder, Self-healing polymer electrolytes for next-generation lithium batteries, Polymers 15 (2023) 1145.
[49] X. Wang, M. Wang, H. Chen, Y. Zhang, B. Niu, L. Tian, D. Long, Dynamically reversible cross-linked polymer electrolytes with highly ionic conductivity for dendrite-free lithium metal batteries, Chem. Eng. J. 496 (2024) 153830.
[50] Y.H. Jo, S. Li, C. Zuo, Y. Zhang, H. Gan, S. Li, L. Yu, D. He, X. Xie, Z. Xue, Self-healing solid polymer electrolyte facilitated by a dynamic cross-linked polymer matrix for lithium-ion batteries, Macromolecules 53 (2020) 1024–1032.
[51] R. Chen, W. Qu, X. Guo, L. Li, F. Wu, The pursuit of solid-state electrolytes for lithium batteries: from comprehensive insight to emerging horizons, Mater. Horiz. 3 (2016) 487–516.
[52] J. Zhu, Z. Zhang, S. Zhao, A.S. Westover, I. Belharouak, P.-F. Cao, Single-ion conducting polymer electrolytes for solid-state lithium–metal batteries: design, performance, and challenges, Adv. Energy Mater. 11 (2021) 2003836.
[53] L. Porcarelli, A.S. Shaplov, F. Bella, J.R. Nair, D. Mecerreyes, C. Gerbaldi, Single-ion conducting polymer electrolytes for lithium metal polymer batteries that operate at ambient temperature, ACS Energy Lett. 1 (2016) 678–682.
[54] H. Lyu, X. Gao, L. Michalek, T. Chen, W. Yu, C.Y.J. Lim, J. Florian, L. Mondonico, W. Zhang, S. Sarkar, P. Zhang, Y. Shi, K.-Y. Lin, S.-L. Liao, X. Zheng, J. Qin, Y. Cui, Z. Bao, Stabilizing all-solid-state Li–S batteries by a polysulfide-repelling and anode-protecting self-segregated trilayer polymer electrolyte, J. Am. Chem. Soc. 148 (2026) 5275–5286.
[55] C. Cao, Y. Li, Y. Feng, C. Peng, Z. Li, W. Feng, A solid-state single-ion polymer electrolyte with ultrahigh ionic conductivity for dendrite-free lithium metal batteries, Energy Storage Mater. 19 (2019) 401–407.
[56] K. Jeong, S. Park, S.-Y. Lee, Revisiting polymeric single lithium-ion conductors as an organic route for all-solid-state lithium ion and metal batteries, J. Mater. Chem. A 7 (2019) 1917–1935.
[57] J.A. Dawson, P. Canepa, T. Famprikis, C. Masquelier, M.S. Islam, Atomic-scale influence of grain boundaries on Li-ion conduction in solid electrolytes for all-solid-state batteries, J. Am. Chem. Soc. 140 (2018) 362–368.
[58] Y. Gao, A.M. Nolan, P. Du, Y. Wu, C. Yang, Q. Chen, Y. Mo, S.-H. Bo, Classical and emerging characterization techniques for investigation of ion transport mechanisms in crystalline fast ionic conductors, Chem. Rev. 120 (2020) 5954–6008.
[59] P. Vadhva, J. Hu, M.J. Johnson, R. Stocker, M. Braglia, D.J.L. Brett, A.J.E. Rettie, Electrochemical impedance spectroscopy for all-solid-state batteries: theory, methods and future outlook, ChemElectroChem 8 (2021) 1930–1947.
[60] S. Yu, D.J. Siegel, Grain boundary contributions to Li-ion transport in the solid electrolyte $Li_7La_3Zr_2O_{12}$ (LLZO), Chem. Mater. 29 (2017) 9639–9647.
[61] S. Breuer, D. Prutsch, Q. Ma, V. Epp, F. Preishuber-Pflügl, F. Tietz, M. Wilkening, Separating bulk from grain boundary Li ion conductivity in the sol–gel prepared solid electrolyte $Li_{1.5}Al_{0.5}Ti_{1.5}(PO_4)_3$, J. Mater. Chem. A 3 (2015) 21343–21350.
[62] E.J. Cheng, A. Sharafi, J. Sakamoto, Intergranular li metal propagation through polycrystalline $Li_{6.25}Al_{0.25}La_3Zr_2O_{12}$ ceramic electrolyte, Electrochim. Acta 223 (2017) 85–91.
[63] E. Milan, M. Pasta, The role of grain boundaries in solid-state li-metal batteries, Mater. Futur. 2 (2022) 013501.
[64] K. McKenna, A. Shluger, The interaction of oxygen vacancies with grain boundaries in monoclinic HfO_2, Appl. Phys. Lett. 95 (2009) 222111.
[65] M. Wilkening, D. Bork, S. Indris, P. Heitjans, Diffusion in amorphous linbo3 studied by ^{7}Li NMR — comparison with the nano- and microcrystalline material, Phys. Chem. Chem. Phys. 4 (2002) 3246–3251.
[66] P. Heitjans, E. Tobschall, M. Wilkening, Ion transport and diffusion in nanocrystalline and glassy ceramics, Eur. Phys. J. Spec. Top. 161 (2008) 97–108.
[67] W.G. Suci, H.K. (Kiwi) Aliwarga, Y.R. Azinuddin, R.B. Setyawati, K.N.R. Stulasti, A. Purwanto, Review of various sulfide electrolyte types for solid-state lithium-ion batteries, Open Eng. 12 (2022) 409–423.
[68] A.K. Mishra, J. Parmar, I. Mukhopadhyay, Comprehensive review on nucleation, growth, and suppression of lithium dendrites in lithium anode batteries, J. Energy Storage 87 (2024) 111421.
[69] Y. Fu, Z. Gu, Q. Gan, Y.-W. Mai, A review on the ionic conductivity and mechanical properties of composite polymer electrolytes (cpes) for lithium batteries: insights from the perspective of polymer/filler composites, Mater. Sci. Eng. R Rep. 160 (2024) 100815.
[70] M.B. Dixit, W. Zaman, N. Hortance, S. Vujic, B. Harkey, F. Shen, W.-Y. Tsai, V. De Andrade, X.C. Chen, N. Balke, K.B. Hatzell, Nanoscale mapping of extrinsic interfaces in hybrid solid electrolytes, Joule 4 (2020) 207–221.
[71] C.-Z. Zhao, X.-Q. Zhang, X.-B. Cheng, R. Zhang, R. Xu, P.-Y. Chen, H.-J. Peng, J.-Q. Huang, Q. Zhang, An anion-immobilized composite electrolyte for dendrite-free lithium metal anodes, Proc. Natl. Acad. Sci. 114 (2017) 11069–11074.
[72] S. Liu, W. Liu, D. Ba, Y. Zhao, Y. Ye, Y. Li, J. Liu, Filler-integrated composite polymer electrolyte for solid-state lithium batteries, Adv. Mater. 35 (2023) 2110423.
[73] F. Zheng, C. Li, Z. Li, X. Cao, H. Luo, J. Liang, X. Zhao, J. Kong, Advanced composite solid electrolytes for lithium batteries: filler dimensional design and ion path optimization, Small 19 (2023) 2206355.
[74] J. Wan, J. Xie, D.G. Mackanic, W. Burke, Z. Bao, Y. Cui, Status, promises, and challenges of nanocomposite solid-state electrolytes for safe and high performance lithium batteries, Mater. Today Nano 4 (2018) 1–16.
[75] J. Zheng, M. Tang, Y.-Y. Hu, Lithium ion pathway within $Li_7La_3Zr_2O_{12}$-polyethylene oxide composite electrolytes, Angew. Chem. Int. Ed. 55 (2016) 12538–12542.
[76] F. Chen, D. Yang, W. Zha, B. Zhu, Y. Zhang, J. Li, Y. Gu, Q. Shen, L. Zhang, D. R. Sadoway, Solid polymer electrolytes incorporating cubic $Li_7La_3Zr_2O_{12}$ for all-solid-state lithium rechargeable batteries, Electrochim. Acta 258 (2017) 1106–1114.
[77] Q. Yang, G. Li, D. Shi, L. Gao, N. Deng, W. Kang, B. Cheng, Composite solid electrolyte with continuous and fast organic–inorganic ion transport highways created by 3D crimped nanofibers@functional ceramic nanowires, Small 19 (2023) 2301521.
[78] H. Yang, J. Bright, B. Chen, P. Zheng, X. Gao, B. Liu, S. Kasani, X. Zhang, N. Wu, Chemical interaction and enhanced interfacial ion transport in a ceramic nanofiber–polymer composite electrolyte for all-solid-state lithium metal batteries, J. Mater. Chem. A 8 (2020) 7261–7272.
[79] M.M.U. Din, M. Häusler, S.M. Fischer, K. Ratzenböck, F.F. Chamasemani, I. Hanghofer, V. Henninge, R. Brunner, C. Slugovc, D. Rettenwander, Role of filler content and morphology in LLZO/PEO membranes, Front. Energy Res. 9 (2021) 711610.
[80] K.-L. Zhang, N. Li, X. Li, J. Huang, H. Chen, S. Jiao, W.-L. Song, Understanding enhanced ionic conductivity in composite solid-state electrolyte in a wide frequency range of 10–2–1010 Hz, Adv. Sci. 9 (2022) 2200213.
[81] D. Brogioli, F. Langer, R. Kun, F. La Mantia, Space-charge effects at the $Li_7La_3Zr_2O_{12}$/poly(ethylene oxide) interface, ACS Appl. Mater. Interfaces 11 (2019) 11999–12007.
[82] W. Liu, S.W. Lee, D. Lin, F. Shi, S. Wang, A.D. Sendek, Y. Cui, Enhancing ionic conductivity in composite polymer electrolytes with well-aligned ceramic nanowires, Nat. Energy 2 (2017) 17035.
[83] T. Yang, J. Zheng, Q. Cheng, Y.-Y. Hu, C.K. Chan, Composite polymer electrolytes with $Li_7La_3Zr_2O_{12}$ garnet-type nanowires as ceramic fillers: mechanism of conductivity enhancement and role of doping and morphology, ACS Appl. Mater. Interfaces 9 (2017) 21773–21780.
[84] W. Liu, N. Liu, J. Sun, P.-C. Hsu, Y. Li, H.-W. Lee, Y. Cui, Ionic conductivity enhancement of polymer electrolytes with ceramic nanowire fillers, Nano Lett. 15 (2015) 2740–2745.
[85] K. Pan, L. Zhang, W. Qian, X. Wu, K. Dong, H. Zhang, S. Zhang, A flexible ceramic/polymer hybrid solid electrolyte for solid-state lithium metal batteries, Adv. Mater. 32 (2020) 2000399.
[86] X. Ma, M. Liu, Q. Wu, X. Guan, F. Wang, H. Liu, J. Xu, Composite electrolytes prepared by improving the interfacial compatibility of organic–inorganic electrolytes for dendrite-free, long-life all-solid lithium metal batteries, ACS Appl. Mater. Interfaces 14 (2022) 53828–53839.
[87] L. Chen, Y. Li, S.-P. Li, L.-Z. Fan, C.-W. Nan, J.B. Goodenough, PEO/garnet composite electrolytes for solid-state lithium batteries: from "ceramic-in-polymer" to "polymer-in-ceramic", Nano Energy 46 (2018) 176–184.
[88] Y. Shan, L. Li, X. Chen, S. Fan, H. Yang, Y. Jiang, Gentle haulers of lithium-ion–nanomolybdenum carbide fillers in solid polymer electrolyte, ACS Energy Lett. 7 (2022) 2289–2296.
[89] S. Chang, Q. Wang, A. Wang, M. Yi, B. Zhu, M. Zhang, Y. Xiao, Y. Hu, X. Wang, Y. Lai, M. Wang, Z. Zhang, Highly efficient ion-transport "polymer-in-ceramic" electrolytes boost stable all-solid-state li metal batteries, J. Colloid Interface Sci. 671 (2024) 477–485.
[90] L. Cheng, W. Chen, M. Kunz, K. Persson, N. Tamura, G. Chen, M. Doeff, Effect of surface microstructure on electrochemical performance of garnet solid electrolytes, ACS Appl. Mater. Interfaces 7 (2015) 2073–2081.
[91] X. Liu, R. Garcia-Mendez, A.R. Lupini, Y. Cheng, Z.D. Hood, F. Han, A. Sharafi, J. C. Idrobo, N.J. Dudney, C. Wang, C. Ma, J. Sakamoto, M. Chi, Local electronic structure variation resulting in Li 'filament' formation within solid electrolytes, Nat. Mater. 20 (2021) 1485–1490.

[92] R.B. Ross, Metallic Materials Specification Handbook, 1992. Glasgow.
[93] L. Stolz, G. Homann, M. Winter, J. Kasnatscheew, The sand equation and its enormous practical relevance for solid-state lithium metal batteries, Mater. Today 44 (2021) 9–14.
[94] X.-R. Chen, Y.-X. Yao, C. Yan, R. Zhang, X.-B. Cheng, Q. Zhang, A diffusion–reaction competition mechanism to tailor lithium deposition for lithium-metal batteries, Angew. Chem. Int. Ed. 59 (2020) 7743–7747.
[95] T. Fuchs, T. Ortmann, J. Becker, C.G. Haslam, M. Ziegler, V.K. Singh, M. Rohnke, B. Mogwitz, K. Peppler, L.F. Nazar, J. Sakamoto, J. Janek, Imaging the microstructure of lithium and sodium metal in anode-free solid-state batteries using electron backscatter diffraction, Nat. Mater. 23 (2024) 1678–1685.
[96] M.R. Nadler, C.P. Kempier, Crystallographic data 186. lithium, Anal. Chem. 31 (1959) 2109, 2109.
[97] M. Yang, Y. Liu, Y. Mo, Lithium crystallization at solid interfaces, Nat. Commun. 14 (2023) 2986.
[98] Y. Liu, X. Xu, M. Sadd, O.O. Kapitanova, V.A. Krivchenko, J. Ban, J. Wang, X. Jiao, Z. Song, J. Song, S. Xiong, A. Matic, Insight into the critical role of exchange current density on electrodeposition behavior of lithium metal, Adv. Sci. 8 (2021) 2003301.
[99] X. Wang, G. Pawar, Y. Li, X. Ren, M. Zhang, B. Lu, A. Banerjee, P. Liu, E.J. Dufek, J.-G. Zhang, J. Xiao, J. Liu, Y.S. Meng, B. Liaw, Glassy Li metal anode for high-performance rechargeable Li batteries, Nat. Mater. 19 (2020) 1339–1345.
[100] R. Koerver, W. Zhang, L. de Biasi, S. Schweidler, A.O. Kondrakov, S. Kolling, T. Brezesinski, P. Hartmann, W.G. Zeier, J. Janek, Chemo-mechanical expansion of lithium electrode materials – on the route to mechanically optimized all-solid-state batteries, Energy Environ. Sci. 11 (2018) 2142–2158.
[101] J. Gu, X. Chen, R. Ma, Z. He, Z. Liang, H. Zhong, Y. Su, J. Shi, Y. Yang, The insight of micro-short circuits caused by electrochemo-mechanical stress crosstalk in all-solid-state Li metal batteries, Energy Storage Mater. 63 (2023) 103052.
[102] Y. Lu, C.-Z. Zhao, H. Yuan, X.-B. Cheng, J.-Q. Huang, Q. Zhang, Critical current density in solid-state lithium metal batteries: mechanism, influences, and strategies, Adv. Funct. Mater. 31 (2021) 2009925.
[103] J. Kasemchainan, S. Zekoll, D. Spencer Jolly, Z. Ning, G.O. Hartley, J. Marrow, P. G. Bruce, Critical stripping current leads to dendrite formation on plating in lithium anode solid electrolyte cells, Nat. Mater. 18 (2019) 1105–1111.
[104] A. Masias, N. Felten, R. Garcia-Mendez, J. Wolfenstine, J. Sakamoto, Elastic, plastic, and creep mechanical properties of lithium metal, J. Mater. Sci. 54 (2019) 2585–2600.
[105] S. Ding, L. Fairgrieve-Park, O. Sendetskyi, M.D. Fleischauer, Compressive creep deformation of lithium foil at varied cell conditions, J. Power Sources 488 (2021) 229404.
[106] N.J.J. de Klerk, M. Wagemaker, Space-charge layers in all-solid-state batteries; important or negligible? ACS Appl. Energy Mater. 1 (2018) 5609–5618.
[107] C. Liu, Z.G. Neale, G. Cao, Understanding electrochemical potentials of cathode materials in rechargeable batteries, Mater. Today 19 (2016) 109–123.
[108] R. Usiskin, J. Maier, Interfacial effects in lithium and sodium batteries, Adv. Energy Mater. 11 (2021) 2001455.
[109] L. Katzenmeier, M. Gößwein, L. Carstensen, J. Sterzinger, M. Ederer, P. Müller-Buschbaum, A. Gagliardi, A.S. Bandarenka, Mass transport and charge transfer through an electrified interface between metallic lithium and solid-state electrolytes, Commun. Chem. 6 (2023) 124.
[110] Y. Li, H. Xu, Q. Ning, S. Li, J. Wang, J. Wang, Z. Hu, J. Tian, X. Li, Y. Han, Y. Zhu, Visualizing structure, growth, and dynamics of Li dendrite in batteries: from atomic to device scales, Adv. Funct. Mater. 34 (2024) 2401361.
[111] J. Scharf, M. Chouchane, D.P. Finegan, B. Lu, C. Redquest, M. Kim, W. Yao, A. A. Franco, D. Gostovic, Z. Liu, M. Riccio, F. Zelenka, J.-M. Doux, Y.S. Meng, Bridging nano- and microscale x-ray tomography for battery research by leveraging artificial intelligence, Nat. Nanotechnol. 17 (2022) 446–459.
[112] F. Tang, Z. Wu, C. Yang, M. Osenberg, A. Hilger, K. Dong, H. Markötter, I. Manke, F. Sun, L. Chen, G. Cui, Synchrotron X-ray tomography for rechargeable battery research: fundamentals, setups and applications, Small Methods 5 (2021) 2100557.
[113] X. Peng, Q. Tu, Y. Zhang, K. Jun, F. Shen, T. Ogunfunmi, Y. Sun, M.C. Tucker, G. Ceder, M.C. Scott, Unraveling Li growth kinetics in solid electrolytes due to electron beam charging, Sci. Adv. 9 (2023) eabq3285.
[114] C. Huang, M.D. Wilson, B. Cline, A. Sivarajah, W. Stolp, M.N. Boone, T. Connolley, C.L.A. Leung, Correlating lithium-ion transport and interfacial lithium microstructure evolution in solid-state batteries during the first cycle, Cell Rep. Phys. Sci. 5 (2024) 101995.
[115] J.S. Lowe, U. Janakiraman, G. Less, R. Kerns, N.S. Muyanja, Using x-ray microscopy to probe failure mechanisms in anode-free cells: an industry perspective, ECS Adv 3 (2024) 040501.
[116] L. Weckelmann, K. Dzieciol, C. König, C.-L. Tsai, A. Windmüller, L. Raijmakers, H. Tempel, H. Kungl, R.-A. Eichel, A novel pressurized operando battery cell for laboratory X-ray computed tomography, Methods Microsc. 2 (2025) 417–430.
[117] S. Dayani, H. Markötter, A. Schmidt, M.P. Widjaja, G. Bruno, Multi-level X-ray computed tomography (XCT) investigations of commercial lithium-ion batteries from cell to particle level, J. Energy Storage 66 (2023) 107453.
[118] D.S. Eastwood, R.S. Bradley, F. Tariq, S.J. Cooper, O.O. Taiwo, J. Gelb, A. Merkle, D.J.L. Brett, N.P. Brandon, P.J. Withers, P.D. Lee, P.R. Shearing, The application of phase contrast X-ray techniques for imaging Li-ion battery electrodes, Nucl. Instrum. Methods Phys. Res. Sect. B Beam Interact. Mater. At. 324 (2014) 118–123.
[119] S. Mayo, M. Endrizzi, X-ray phase contrast methods, Handb. Adv. Nondestruct. Eval (2019) 1053–1093.
[120] H. Dierks, J. Wallentin, Experimental optimization of X-ray propagation-based phase contrast imaging geometry, Opt. Express 28 (2020) 29562–29575.
[121] G. McConohy, X. Xu, T. Cui, E. Barks, S. Wang, E. Kaeli, C. Melamed, X.W. Gu, W. C. Chueh, Mechanical regulation of lithium intrusion probability in garnet solid electrolytes, Nat. Energy 8 (2023) 241–250.
[122] L. Zhao, M. Feng, C. Wu, L. Guo, Z. Chen, S. Risal, Q. Ai, J. Lou, Z. Fan, Y. Qi, Y. Yao, Imaging the evolution of lithium-solid electrolyte interface using operando scanning electron microscopy, Nat. Commun. 16 (2025) 4283.
[123] T. Wang, B. Chen, Y. Liu, Z. Song, Z. Wang, Y. Chen, Q. Yu, J. Wen, Y. Dai, Q. Kang, F. Pei, R. Xu, W. Luo, Y. Huang, Fatigue of Li metal anode in solid-state batteries, Science 388 (2025) 311–316.
[124] J.-M. Doux, Y. Yang, D.H.S. Tan, H. Nguyen, E.A. Wu, X. Wang, A. Banerjee, Y. S. Meng, Pressure effects on sulfide electrolytes for all solid-state batteries, J. Mater. Chem. A 8 (2020) 5049–5055.
[125] D.L.R. Melvin, M. Siniscalchi, D. Spencer-Jolly, B. Hu, Z. Ning, S. Zhang, J. Bu, S. Marathe, A. Bonnin, J. Ihli, G.J. Rees, P.S. Grant, C.W. Monroe, T.J. Marrow, G. Li, P.G. Bruce, High plating currents without dendrites at the interface between a lithium anode and solid electrolyte, Nat. Energy 10 (2025) 1205–1214.
[126] Z. Ju, H. Yuan, O. Sheng, T. Liu, J. Nai, Y. Wang, Y. Liu, X. Tao, Cryo-electron microscopy for unveiling the sensitive battery materials, Small Sci. 1 (2021) 2100055.
[127] A. Mikitisin, H. Ditler, M. Schütte, Correlative electron and X-ray microscopy: a new lens for sodium-ion battery research, Methods Microsc. 2 (2025) 329–340.
[128] E.P. Alsaç, D.L. Nelson, S.G. Yoon, K.A. Cavallaro, C. Wang, S.E. Sandoval, U. D. Eze, W.J. Jeong, M.T. McDowell, Characterizing electrode materials and interfaces in solid-state batteries, Chem. Rev. 125 (2025) 2009–2119.
[129] J. Gu, Z. Liang, J. Shi, Y. Yang, Electrochemo-mechanical stresses and their measurements in sulfide-based all-solid-state batteries: a review, Adv. Energy Mater. 13 (2023) 2203153.
[130] C. Chen, M. Jiang, T. Zhou, L. Raijmakers, E. Vezhlev, B. Wu, T.U. Schülli, D. L. Danilov, Y. Wei, R.-A. Eichel, P.H.L. Notten, Interface aspects in all-solid-state Li-based batteries reviewed, Adv. Energy Mater. 11 (2021) 2003939.
[131] V. Reisecker, F. Flatscher, L. Porz, C. Fincher, J. Todt, I. Hanghofer, V. Hennige, M. Linares-Moreau, P. Falcaro, S. Ganschow, S. Wenner, Y.-M. Chiang, J. Keckes, J. Fleig, D. Rettenwander, Effect of pulse-current-based protocols on the lithium dendrite formation and evolution in all-solid-state batteries, Nat. Commun. 14 (2023) 2432.
[132] J. Jiao, G. Lai, L. Zhao, J. Lu, Q. Li, X. Xu, Y. Jiang, Y.-B. He, C. Ouyang, F. Pan, H. Li, J. Zheng, Self-healing mechanism of lithium in lithium metal, Adv. Sci. 9 (2022) 2105574.
[133] M. Klimpel, H. Zhang, M.V. Kovalenko, K.V. Kravchyk, Standardizing critical current density measurements in lithium garnets, Commun. Chem. 6 (2023) 192.
[134] A. Morchhale, Z. Tang, R. Ghahremani, R. Farahati, J.-H. Kim, Re-evaluating critical current density in solid-state batteries: challenges and proposing an alternative, J. Power Sources 624 (2024) 235605.
[135] J.A. Lewis, C. Lee, Y. Liu, S.Y. Han, D. Prakash, E.J. Klein, H.-W. Lee, M. T. McDowell, Role of areal capacity in determining short circuiting of sulfide-based solid-state batteries, ACS Appl. Mater. Interfaces 14 (2022) 4051–4060.
[136] S. Sarkar, V. Thangadurai, Critical current densities for high-performance all-solid-state Li-metal batteries: fundamentals, mechanisms, interfaces, materials, and applications, ACS Energy Lett. 7 (2022) 1492–1527.
[137] K. Li, J. Huang, X. Qu, G. Fu, X. Chen, W. Shen, Y. Lin, Void evolution at the Li/LLZO interface: stack pressure and operating temperature-driven creep effect, ACS Appl. Mater. Interfaces 17 (2025) 3146–3162.
[138] J.-M. Doux, H. Nguyen, D.H.S. Tan, A. Banerjee, X. Wang, E.A. Wu, C. Jo, H. Yang, Y.S. Meng, Stack pressure considerations for room-temperature all-solid-state lithium metal batteries, Adv. Energy Mater. 10 (2020) 1903253.
[139] S. Wang, W. Zhang, X. Chen, D. Das, R. Ruess, A. Gautam, F. Walther, S. Ohno, R. Koerver, Q. Zhang, W.G. Zeier, F.H. Richter, C.-W. Nan, J. Janek, Influence of crystallinity of lithium thiophosphate solid electrolytes on the performance of solid-state batteries, Adv. Energy Mater. 11 (2021) 2100654.
[140] J. Gu, R. Xu, B. Chen, J. Zhou, NMC811-Li_6PS_5Cl-Li/in all-solid-state battery capacity attenuation based on temperature-pressure-electrochemical coupling model, J. Electrochem. Soc. 170 (2023) 040504.
[141] F. Aguesse, W. Manalastas, L. Buannic, J.M. Lopez del Amo, G. Singh, A. Llordés, J. Kilner, Investigating the dendritic growth during full cell cycling of garnet electrolyte in direct contact with Li metal, ACS Appl. Mater. Interfaces 9 (2017) 3808–3816.
[142] Y. Jin, K. Liu, J. Lang, D. Zhuo, Z. Huang, C. Wang, H. Wu, Y. Cui, An intermediate temperature garnet-type solid electrolyte-based molten lithium battery for grid energy storage, Nat. Energy 3 (2018) 732–738.
[143] B. Kinzer, A.L. Davis, T. Krauskopf, H. Hartmann, W.S. LePage, E. Kazyak, J. Janek, N.P. Dasgupta, J. Sakamoto, Operando analysis of the molten li|llzo interface: understanding how the physical properties of Li affect the critical current density, Matter 4 (2021) 1947–1961.
[144] S. Zhou, M. Li, P. Wang, L. Cheng, L. Chen, Y. Huang, B. Cao, S. Yu, Q. Liu, J. Wei, Liquid metal as an efficient protective layer for lithium metal anodes in all-solid-state batteries, Carbon Energy 6 (2024) e462.
[145] F. Pei, L. Wu, Y. Zhang, Y. Liao, Q. Kang, Y. Han, H. Zhang, Y. Shen, H. Xu, Z. Li, Y. Huang, Interfacial self-healing polymer electrolytes for long-cycle solid-state lithium-sulfur batteries, Nat. Commun. 15 (2024) 351.
[146] P. Jaumaux, Q. Liu, D. Zhou, X. Xu, T. Wang, Y. Wang, F. Kang, B. Li, G. Wang, Deep-eutectic-solvent-based self-healing polymer electrolyte for safe and long-life lithium-metal batteries, Angew. Chem. Int. Ed. 59 (2020) 9134–9142.

[147] K. Deng, S. Zhou, Z. Xu, M. Xiao, Y. Meng, A high ion-conducting, self-healing and nonflammable polymer electrolyte with dynamic imine bonds for dendrite-free lithium metal batteries, Chem. Eng. J. 428 (2022) 131224.
[148] B. Zhou, D. He, J. Hu, Y. Ye, H. Peng, X. Zhou, X. Xie, Z. Xue, A flexible, self-healing and highly stretchable polymer electrolyte via quadruple hydrogen bonding for lithium-ion batteries, J. Mater. Chem. A 6 (2018) 11725–11733.
[149] W. Wang, J. Wang, C. Lin, H. Ruan, Modeling of void-mediated cracking and lithium penetration in all-solid-state batteries, Adv. Funct. Mater. 33 (2023) 2303484.
[150] T. Krauskopf, H. Hartmann, W.G. Zeier, J. Janek, Toward a fundamental understanding of the lithium metal anode in solid-state batteries—an electrochemo-mechanical study on the garnet-type solid electrolyte $Li_{6.25}Al_{0.25}La_3Zr_2O_{12}$, ACS Appl. Mater. Interfaces 11 (2019) 14463–14477.
[151] C.-L. Tsai, T. Lan, C. Dellen, Y. Ling, Q. Ma, D. Fattakhova-Rohlfing, O. Guillon, F. Tietz, Dendrite-tolerant all-solid-state sodium batteries and an important mechanism of metal self-diffusion, J. Power Sources 476 (2020) 228666.
[152] Y. Wang, T. Liu, J. Kumar, Effect of pressure on lithium metal deposition and stripping against sulfide-based solid electrolytes, ACS Appl. Mater. Interfaces 12 (2020) 34771–34776.
[153] Y. Lu, C.-Z. Zhao, J.-K. Hu, S. Sun, H. Yuan, Z.-H. Fu, X. Chen, J.-Q. Huang, M. Ouyang, Q. Zhang, The void formation behaviors in working solid-state Li metal batteries, Sci. Adv. 8 (2022) eadd0510.
[154] S.S. Shishvan, N.A. Fleck, V.S. Deshpande, The initiation of void growth during stripping of Li electrodes in solid electrolyte cells, J. Power Sources 488 (2021) 229437.
[155] S.L. Dreyer, A. Kondrakov, J. Janek, T. Brezesinski, In situ analysis of gas evolution in liquid- and solid-electrolyte-based batteries with current and next-generation cathode materials, J. Mater. Res. 37 (2022) 3146–3168.
[156] C. Sångeland, B. Sun, D. Brandell, E.J. Berg, J. Mindemark, Decomposition of carbonate-based electrolytes: differences and peculiarities for liquids vs. polymers observed using operando gas analysis, Batter. Supercaps 4 (2021) 785–790.
[157] X. Zhang, C. Luo, N. Menga, H. Zhang, Y. Li, S.-P. Zhu, Pressure and polymer selections for solid-state batteries investigated with high-throughput simulations, Cell Rep. Phys. Sci. 4 (2023) 101328.
[158] S. Hu, P. Xu, L.S. de Vasconcelos, L. Stanciu, H. Ni, K. Zhao, Elastic modulus, hardness, and fracture toughness of $Li_{6.4}La_3Zr_{1.4}Ta_{0.6}O_{12}$ solid electrolyte, Chin. Phys. Lett. 38 (2021) 098401.
[159] P. Gorai, T. Famprikis, B. Singh, V. Stevanović, P. Canepa, Devil is in the defects: electronic conductivity in solid electrolytes, Chem. Mater. 33 (2021) 7484–7498.
[160] J. Biao, C. Bai, J. Ma, M. Liu, F. Kang, Y. Cao, Y.-B. He, Perspectives on Li dendrite penetration in $Li_7La_3Zr_2O_{12}$-based solid-state electrolytes and batteries: materials, interfaces, and charge transfer, Adv. Energy Mater. 14 (2024) 2303128.
[161] F. Han, A.S. Westover, J. Yue, X. Fan, F. Wang, M. Chi, D.N. Leonard, N. J. Dudney, H. Wang, C. Wang, High electronic conductivity as the origin of lithium dendrite formation within solid electrolytes, Nat. Energy 4 (2019) 187–196.
[162] T. Thompson, S. Yu, L. Williams, R.D. Schmidt, R. Garcia-Mendez, J. Wolfenstine, J.L. Allen, E. Kioupakis, D.J. Siegel, J. Sakamoto, Electrochemical window of the Li-ion solid electrolyte $Li_7La_3Zr_2O_{12}$, ACS Energy Lett. 2 (2017) 462–468.
[163] B. Shao, Y. Huang, F. Han, Electronic conductivity of lithium solid electrolytes, Adv. Energy Mater. 13 (2023) 2204098.
[164] Y. Song, L. Yang, W. Zhao, Z. Wang, Y. Zhao, Z. Wang, Q. Zhao, H. Liu, F. Pan, Revealing the short-circuiting mechanism of garnet-based solid-state electrolyte, Adv. Energy Mater. 9 (2019) 1900671.
[165] J.A. Lewis, F.J.Q. Cortes, M.G. Boebinger, J. Tippens, T.S. Marchese, N. Kondekar, X. Liu, M. Chi, M.T. McDowell, Interphase morphology between a solid-state electrolyte and lithium controls cell failure, ACS Energy Lett. 4 (2019) 591–599.
[166] H. Liu, Y. Chen, P.-H. Chien, G. Amouzandeh, D. Hou, E. Truong, I.P. Oyekunle, J. Bhagu, S.W. Holder, H. Xiong, P.L. Gor'kov, J.T. Rosenberg, S.C. Grant, Y.-Y. Hu, Dendrite formation in solid-state batteries arising from lithium plating and electrolyte reduction, Nat. Mater. 24 (2025) 581–588.
[167] C. Zhu, T. Fuchs, S.A.L. Weber, F.H. Richter, G. Glasser, F. Weber, H.-J. Butt, J. Janek, R. Berger, Understanding the evolution of lithium dendrites at $Li_{6.25}Al_{0.25}La_3Zr_2O_{12}$ grain boundaries via operando microscopy techniques, Nat. Commun. 14 (2023) 1300.
[168] A. Sharafi, C.G. Haslam, R.D. Kerns, J. Wolfenstine, J. Sakamoto, Controlling and correlating the effect of grain size with the mechanical and electrochemical properties of $Li_7La_3Zr_2O_{12}$ solid-state electrolyte, J. Mater. Chem. A 5 (2017) 21491–21504.
[169] M. Sun, T. Liu, Y. Yuan, M. Ling, N. Xu, Y. Liu, L. Yan, H. Li, C. Liu, Y. Lu, Y. Shi, Y. He, Y. Guo, X. Tao, C. Liang, J. Lu, Visualizing lithium dendrite formation within solid-state electrolytes, ACS Energy Lett. 6 (2021) 451–458.
[170] R. Raj, J. Wolfenstine, Current limit diagrams for dendrite formation in solid-state electrolytes for Li-ion batteries, J. Power Sources 343 (2017) 119–126.
[171] B. Zhang, B. Yuan, X. Yan, X. Han, J. Zhang, H. Tan, C. Wang, P. Yan, H. Gao, Y. Liu, Atomic mechanism of lithium dendrite penetration in solid electrolytes, Nat. Commun. 16 (2025) 1906.
[172] K.J. Harry, X. Liao, D.Y. Parkinson, A.M. Minor, N.P. Balsara, Electrochemical deposition and stripping behavior of lithium metal across a rigid block copolymer electrolyte membrane, J. Electrochem. Soc. 162 (2015) A2699.
[173] A. Parejiya, R. Amin, R. Essehli, D.L.I. Wood, I. Belharouak, Electrochemical healing of dendrites in garnet-based solid electrolytes, ACS Energy Lett. 5 (2020) 3368–3373.
[174] W. Ping, C. Wang, Z. Lin, E. Hitz, C. Yang, H. Wang, L. Hu, Reversible short-circuit behaviors in garnet-based solid-state batteries, Adv. Energy Mater. 10 (2020) 2000702.
[175] Y. Zhu, X. He, Y. Mo, Origin of outstanding stability in the lithium solid electrolyte materials: insights from thermodynamic analyses based on first-principles calculations, ACS Appl. Mater. Interfaces 7 (2015) 23685–23693.
[176] S. Wang, H. Xu, W. Li, A. Dolocan, A. Manthiram, Interfacial chemistry in solid-state batteries: formation of interphase and its consequences, J. Am. Chem. Soc. 140 (2018) 250–257.
[177] S. Lorger, R. Usiskin, J. Maier, Transport and charge carrier chemistry in lithium oxide, J. Electrochem. Soc. 166 (2019) A2215.
[178] J.A. Lewis, F.J.Q. Cortes, Y. Liu, J.C. Miers, A. Verma, B.S. Vishnugopi, J. Tippens, D. Prakash, T.S. Marchese, S.Y. Han, C. Lee, P.P. Shetty, H.-W. Lee, P. Shevchenko, F. De Carlo, C. Saldana, P.P. Mukherjee, M.T. McDowell, Linking void and interphase evolution to electrochemistry in solid-state batteries using operando X-ray tomography, Nat. Mater. 20 (2021) 503–510.
[179] F. Sun, C. Wang, M. Osenberg, K. Dong, S. Zhang, C. Yang, Y. Wang, A. Hilger, J. Zhang, S. Dong, H. Markötter, I. Manke, G. Cui, Clarifying the electro-chemo-mechanical coupling in $Li_{10}SnP_2S_{12}$ based all-solid-state batteries, Adv. Energy Mater. 12 (2022) 2103714.
[180] M. Golozar, A. Paolella, H. Demers, S. Bessette, M. Lagacé, P. Bouchard, A. Guerfi, R. Gauvin, K. Zaghib, In situ observation of solid electrolyte interphase evolution in a lithium metal battery, Commun. Chem. 2 (2019) 131.
[181] Y. Xiao, Y. Wang, S.-H. Bo, J.C. Kim, L.J. Miara, G. Ceder, Understanding interface stability in solid-state batteries, Nat. Rev. Mater. 5 (2020) 105–126.
[182] Z. Gu, D. Song, S. Luo, H. Liu, X. Sun, L. Zhu, W. Ma, X. Zhang, Insights into the anode-initiated and grain boundary-initiated mechanisms for dendrite formation in all-solid-state lithium metal batteries, Adv. Energy Mater. 13 (2023) 2302945.
[183] S. Smetaczek, E. Pycha, J. Ring, M. Siebenhofer, S. Ganschow, S. Berendts, A. Nenning, M. Kubicek, D. Rettenwander, A. Limbeck, J. Fleig, Investigating the electrochemical stability of $Li_7La_3Zr_2O_{12}$ solid electrolytes using field stress experiments, J. Mater. Chem. A 9 (2021) 15226–15237.
[184] Y. Benabed, A. Vanacker, G. Foran, S. Rousselot, G. Hautier, M. Dollé, Solving the $Li_7La_3Zr_2O_{12}$ electrochemical stability window puzzle, Mater. Today Energy 35 (2023) 101320.
[185] C. Wu, J. Lou, J. Zhang, Z. Chen, A. Kakar, B. Emley, Q. Ai, H. Guo, Y. Liang, J. Lou, Y. Yao, Z. Fan, Current status and future directions of all-solid-state batteries with lithium metal anodes, sulfide electrolytes, and layered transition metal oxide cathodes, Nano Energy 87 (2021) 106081.
[186] J. Park, T. Watanabe, K. Yamamoto, T. Uchiyama, T. Takami, A. Sakuda, A. Hayashi, M. Tatsumisago, Y. Uchimoto, Unique Li deposition behavior in Li_3PS_4 solid electrolyte observed via operando X-ray computed tomography, Chem. Commun. 59 (2023) 7799–7802.
[187] J. Tippens, J.C. Miers, A. Afshar, J.A. Lewis, F.J.Q. Cortes, H. Qiao, T.S. Marchese, C.V. Di Leo, C. Saldana, M.T. McDowell, Visualizing chemomechanical degradation of a solid-state battery electrolyte, ACS Energy Lett. 4 (2019) 1475–1483.
[188] C.F.N. Marchiori, R.P. Carvalho, M. Ebadi, D. Brandell, C.M. Araujo, Understanding the electrochemical stability window of polymer electrolytes in solid-state batteries from atomic-scale modeling: the role of Li-ion salts, Chem. Mater. 32 (2020) 7237–7246.
[189] T.K. Schwietert, V.A. Arszelewska, C. Wang, C. Yu, A. Vasileiadis, N.J.J. de Klerk, J. Hageman, T. Hupfer, I. Kerkamm, Y. Xu, E. van der Maas, E.M. Kelder, S. Ganapathy, M. Wagemaker, Clarifying the relationship between redox activity and electrochemical stability in solid electrolytes, Nat. Mater. 19 (2020) 428–435.
[190] T.K. Schwietert, A. Vasileiadis, M. Wagemaker, First-principles prediction of the electrochemical stability and reaction mechanisms of solid-state electrolytes, JACS Au 1 (2021) 1488–1496.
[191] C. Zor, S.J. Turrell, M.S. Uyanik, S. Afyon, Lithium plating and stripping: toward anode-free solid-state batteries, Adv. Energy Sustain. Res. 5 (2024) 2300001.
[192] Y. Li, X. Chen, A. Dolocan, Z. Cui, S. Xin, L. Xue, H. Xu, K. Park, J.B. Goodenough, Garnet electrolyte with an ultralow interfacial resistance for Li-metal batteries, J. Am. Chem. Soc. 140 (2018) 6448–6455.
[193] Y. Guo, J. Cheng, Z. Zeng, Y. Li, H. Zhang, D. Li, L. Ci, Li2CO3: insights into its blocking effect on Li-ion transfer in garnet composite electrolytes, ACS Appl. Energy Mater. 5 (2022) 2853–2861.
[194] S. Heo, D. Lee, K. Kim, Y. Kim, D.-J. Yun, S. Park, J. Lee, S. Kim, J.-S. Kim, S. Park, Short-circuit mechanism induced by crack propagation spurred by inhomogeneous electric field in garnet-based solid electrolyte, J. Power Sources 510 (2021) 230389.
[195] N. Seitzman, H. Guthrey, D.B. Sulas, H.A.S. Platt, M. Al-Jassim, S. Pylypenko, Toward all-solid-state lithium batteries: three-dimensional visualization of lithium migration in β-Li_3PS_4 ceramic electrolyte, J. Electrochem. Soc. 165 (2018) A3732.
[196] F. Mo, J. Ruan, S. Sun, Z. Lian, S. Yang, X. Yue, Y. Song, Y.-N. Zhou, F. Fang, G. Sun, S. Peng, D. Sun, Inside or outside: origin of lithium dendrite formation of all solid-state electrolytes, Adv. Energy Mater. 9 (2019) 1902123.
[197] S. Hao, S.R. Daemi, T.M.M. Heenan, W. Du, C. Tan, M. Storm, C. Rau, D.J.L. Brett, P.R. Shearing, Tracking lithium penetration in solid electrolytes in 3D by in-situ synchrotron X-ray computed tomography, Nano Energy 82 (2021) 105744.
[198] Z. Ning, D.S. Jolly, G. Li, R. De Meyere, S.D. Pu, Y. Chen, J. Kasemchainan, J. Ihli, C. Gong, B. Liu, D.L.R. Melvin, A. Bonnin, O. Magdysyuk, P. Adamson, G. O. Hartley, C.W. Monroe, T.J. Marrow, P.G. Bruce, Visualizing plating-induced cracking in lithium-anode solid-electrolyte cells, Nat. Mater. 20 (2021) 1121–1129.
[199] G. Bucci, J. Christensen, Modeling of lithium electrodeposition at the lithium/ceramic electrolyte interface: the role of interfacial resistance and surface defects, J. Power Sources 441 (2019) 227186.

[200] H. Wang, H. Gao, X. Chen, J. Zhu, W. Li, Z. Gong, Y. Li, M.-S. Wang, Y. Yang, Linking the defects to the formation and growth of Li dendrite in all-solid-state batteries, Adv. Energy Mater. 11 (2021) 2102148.

[201] Y. Takase, M. Kodama, R. Iwamura, H. Kawakami, K. Aotani, Y. Aihara, S. Hirai, Effects of solid electrolyte particle size and silver-carbon interlayer on lithium deposition in all-solid-state lithium-metal batteries, Electrochimica Acta 498 (2024) 144670.

[202] Y. Sakka, H. Yamashige, A. Watanabe, A. Takeuchi, M. Uesugi, K. Uesugi, Y. Orikasa, Pressure dependence on the three-dimensional structure of a composite electrode in an all-solid-state battery, J. Mater. Chem. A 10 (2022) 16602–16609.

[203] M. Otoyama, M. Suyama, C. Hotehama, H. Kowada, Y. Takeda, K. Ito, A. Sakuda, M. Tatsumisago, A. Hayashi, Visualization and control of chemically induced crack formation in all-solid-state lithium-metal batteries with sulfide electrolyte, ACS Appl. Mater. Interface 13 (2021) 5000–5007.

[204] J. Gu, X. Chen, Z. He, Z. Liang, Y. Lin, J. Shi, Y. Yang, Decoding internal stress-induced micro-short circuit events in sulfide-based all-solid-state Li-metal batteries via operando pressure measurements, Adv. Energy Mater. 13 (2023) 2302643.

[205] Z. Ning, G. Li, D.L.R. Melvin, Y. Chen, J. Bu, D. Spencer-Jolly, J. Liu, B. Hu, X. Gao, J. Perera, C. Gong, S.D. Pu, S. Zhang, B. Liu, G.O. Hartley, A.J. Bodey, R. I. Todd, P.S. Grant, D.E.J. Armstrong, T.J. Marrow, C.W. Monroe, P.G. Bruce, Dendrite initiation and propagation in lithium metal solid-state batteries, Nature 618 (2023) 287–293.

[206] D. Cao, K. Zhang, W. Li, Y. Zhang, T. Ji, X. Zhao, E. Cakmak, J. Zhu, Y. Cao, H. Zhu, Nondestructively visualizing and understanding the mechano-electro-chemical origins of "soft short" and "creeping" in all-solid-state batteries, Adv. Funct. Mater. 33 (2023) 2307998.

[207] B. Hu, S. Zhang, Z. Ning, D. Spencer-Jolly, D.L.R. Melvin, X. Gao, J. Perera, S. D. Pu, G.J. Rees, L. Wang, L. Yang, H. Gao, S. Marathe, G. Burca, T.J. Marrow, P. G. Bruce, Deflecting lithium dendritic cracks in multi-layered solid electrolytes, Joule 8 (2024) 2623–2638.

[208] M. Kodama, S. Komiyama, A. Ohashi, N. Horikawa, K. Kawamura, S. Hirai, High-pressure in situ X-ray computed tomography and numerical simulation of sulfide solid electrolyte, J. Power Sources 462 (2020) 228160.

[209] S. Hao, S.R. Daemi, T.M.M. Heenan, W. Du, M. Storm, M. Al-Hada, C. Rau, D.J. L. Brett, P.R. Shearing, Fast degradation of solid electrolyte in initial cycling processes, tracked in 3D by synchrotron X-ray computed tomography, ACS Nano 19 (2025) 20516–20525.

[210] S. Hao, J.J. Bailey, F. Iacoviello, J. Bu, P.S. Grant, D.J.L. Brett, P.R. Shearing, 3D imaging of lithium protrusions in solid-state lithium batteries using X-ray computed tomography, Adv. Funct. Mater. 31 (2021) 2007564.

[211] M. Kodama, N. Uno, Y. Takase, O. Aoki, R. Iwamura, T. Kotaka, K. Aotani, S. Hirai, X-ray computed tomography analysis of lithium deposition in all-solid-state lithium-metal batteries with carbon interlayers bonded through various processes, J. Power Sources Adv. 26 (2024) 100142.

[212] Hütte, Springer, Berlin, Heidelberg, 1991, https://doi.org/10.1007/978-3-662-12030-9.

[213] Z. Ahmad, T. Xie, C. Maheshwari, J.C. Grossman, V. Viswanathan, Machine learning enabled computational screening of inorganic solid electrolytes for suppression of dendrite formation in lithium metal anodes, ACS Cent. Sci. 4 (2018) 996–1006.

[214] L. Porz, T. Swamy, B.W. Sheldon, D. Rettenwander, T. Frömling, H.L. Thaman, S. Berendts, R. Uecker, W.C. Carter, Y.-M. Chiang, Mechanism of lithium metal penetration through inorganic solid electrolytes, Adv. Energy Mater. 7 (2017) 1701003.

[215] J.F. Nonemacher, Y. Arinicheva, G. Yan, M. Finsterbusch, M. Krüger, J. Malzbender, Fracture toughness of single grains and polycrystalline $Li_7La_3Zr_2O_{12}$ electrolyte material based on a pillar splitting method, J. Eur. Ceram. Soc. 40 (2020) 3057–3064.

[216] F. Flatscher, M. Philipp, S. Ganschow, H.M.R. Wilkening, D. Rettenwander, The natural critical current density limit for $Li_7La_3Zr_2O_{12}$ garnets, J. Mater. Chem. A 8 (2020) 15782–15788.

[217] C. Monroe, J. Newman, The effect of interfacial deformation on electrodeposition kinetics, J. Electrochem. Soc. 151 (2004) A880.

[218] C. Monroe, J. Newman, The impact of elastic deformation on deposition kinetics at lithium/polymer interfaces, J. Electrochem. Soc. 152 (2005) A396.

[219] C. Yuan, W. Lu, J. Xu, Unlocking the electrochemical–mechanical coupling behaviors of dendrite growth and crack propagation in all-solid-state batteries, Adv. Energy Mater. 11 (2021) 2101807.

[220] W. Manalastas, J. Rikarte, R.J. Chater, R. Brugge, A. Aguadero, L. Buannic, A. Llordés, F. Aguesse, J. Kilner, Mechanical failure of garnet electrolytes during Li electrodeposition observed by in-operando microscopy, J. Power Sources 412 (2019) 287–293.

[221] J. Hu, Z. Sun, Y. Gao, P. Li, Y. Wu, S. Chen, R. Wang, N. Li, W. Yang, Y. Shen, S.-H. Bo, 3D stress mapping reveals the origin of lithium-deposition heterogeneity in solid-state lithium-metal batteries, Cell Rep. Phys. Sci. 3 (2022) 100938.

[222] M. Cronau, M. Szabo, C. König, T.B. Wassermann, B. Roling, How to measure a reliable ionic conductivity? The stack pressure dilemma of microcrystalline sulfide-based solid electrolytes, ACS Energy Lett. 6 (2021) 3072–3077.

[223] Y. Qi, C. Ban, S.J. Harris, A new general paradigm for understanding and preventing Li metal penetration through solid electrolytes, Joule 4 (2020) 2599–2608.

[224] P. Žguns, B. Yildiz, Strain sensitivity of Li-ion conductivity in β-Li_3PS_4 solid electrolyte, PRX Energy 1 (2022) 023003.

[225] T. Mezaki, Y. Kuronuma, I. Oikawa, A. Kamegawa, H. Takamura, Li-ion conductivity and phase stability of ca-doped $LiBH_4$ under high pressure, Inorg. Chem. 55 (2016) 10484–10489.

[226] H. Wang, M. Yu, Y. Wang, Z. Feng, Y. Wang, X. Lü, J. Zhu, Y. Ren, C. Liang, *In-situ* investigation of pressure effect on structural evolution and conductivity of Na_3SbS_4 superionic conductor, J. Power Sources 401 (2018) 111–116.

[227] Y. Inaguma, J. Yu, Y.-J. Shan, M. Itoh, T. Nakamuraa, The effect of the hydrostatic pressure on the ionic conductivity in a perovskite lanthanum lithium titanate, J. Electrochem. Soc. 142 (1995) L8.

[228] T. Famprikis, Ö.U. Kudu, J.A. Dawson, P. Canepa, F. Fauth, E. Suard, M. Zbiri, D. Dambournet, O.J. Borkiewicz, H. Bouyanfif, S.P. Emge, S. Cretu, J.-N. Chotard, C.P. Grey, W.G. Zeier, M.S. Islam, C. Masquelier, Under pressure: mechanochemical effects on structure and ion conduction in the sodium-ion solid electrolyte Na_3PS_4, J. Am. Chem. Soc. 142 (2020) 18422–18436.

[229] P. Roering, G.M. Overhoff, K.L. Liu, M. Winter, G. Brunklaus, External pressure in polymer-based lithium metal batteries: an often-neglected criterion when evaluating cycling performance? ACS Appl. Mater. Interfaces 16 (2024) 21932–21942.

[230] A. Manuel Stephan, K.S. Nahm, Review on composite polymer electrolytes for lithium batteries, Polymer 47 (2006) 5952–5964.

[231] M.J. Counihan, D.J. Powers, P. Barai, S. Hu, T. Zagorac, Y. Zhou, J. Lee, J. G. Connell, K.S. Chavan, I.S. Gilmore, L. Hanley, V. Srinivasan, Y. Zhang, S. Tepavcevic, Understanding the influence of $Li_7La_3Zr_2O_{12}$ nanofibers on critical current density and coulombic efficiency in composite polymer electrolytes, ACS Appl. Mater. Interfaces 15 (2023) 26047–26059.

[232] H. Huo, Y. Chen, J. Luo, X. Yang, X. Guo, X. Sun, Rational design of hierarchical "ceramic-in-polymer" and "polymer-in-ceramic" electrolytes for dendrite-free solid-state batteries, Adv. Energy Mater. 9 (2019) 1804004.

[233] A. Maity, A. Svirinovsky-Arbeli, Y. Buganim, C. Oppenheim, M. Leskes, Tracking dendrites and solid electrolyte interphase formation with dynamic nuclear polarization—Nmr spectroscopy, Nat. Commun. 15 (2024) 9956.

[234] J.H. Cho, K. Kim, S. Chakravarthy, X. Xiao, J.L.M. Rupp, B.W. Sheldon, An investigation of chemo-mechanical phenomena and Li metal penetration in all-solid-state lithium metal batteries using *in situ* optical curvature measurements, Adv. Energy Mater. 12 (2022) 2200369.

[235] C. Yuan, X. Gao, Y. Jia, W. Zhang, Q. Wu, J. Xu, Coupled crack propagation and dendrite growth in solid electrolyte of all-solid-state battery, Nano Energy 86 (2021) 106057.

[236] S. Lou, Q. Liu, F. Zhang, Q. Liu, Z. Yu, T. Mu, Y. Zhao, J. Borovilas, Y. Chen, M. Ge, X. Xiao, W.-K. Lee, G. Yin, Y. Yang, X. Sun, J. Wang, Insights into interfacial effect and local lithium-ion transport in polycrystalline cathodes of solid-state batteries, Nat. Commun. 11 (2020) 5700.

[237] Y. Zheng, S. Zhang, J. Ma, F. Sun, M. Osenberg, A. Hilger, H. Markötter, F. Wilde, I. Manke, Z. Hu, G. Cui, Codependent failure mechanisms between cathode and anode in solid state lithium metal batteries: mediated by uneven ion flux, Sci. Bull. 68 (2023) 813–825.

[238] J. Li, Y. Cai, H. Wu, Z. Yu, X. Yan, Q. Zhang, T.Z. Gao, K. Liu, X. Jia, Z. Bao, Polymers in lithium-ion and lithium metal batteries, Adv. Energy Mater. 11 (2021) 2003239.

[239] J.F. Snyder, R.H. Carter, E.D. Wetzel, Electrochemical and mechanical behavior in mechanically robust solid polymer electrolytes for use in multifunctional structural batteries, Chem. Mater. 19 (2007) 3793–3801.

[240] H. Gao, X. Ai, H. Wang, W. Li, P. Wei, Y. Cheng, S. Gui, H. Yang, Y. Yang, M.-S. Wang, Visualizing the failure of solid electrolyte under GPa-level interface stress induced by lithium eruption, Nat. Commun. 13 (2022) 5050.

[241] X. Hu, Z. Zhang, X. Zhang, Y. Wang, X. Yang, X. Wang, M. Fayena-Greenstein, H. A. Yehezkel, S. Langford, D. Zhou, B. Li, G. Wang, D. Aurbach, External-pressure–electrochemistry coupling in solid-state lithium metal batteries, Nat. Rev. Mater. 9 (2024) 305–320.

[242] M.J. Counihan, K.S. Chavan, P. Barai, D.J. Powers, Y. Zhang, V. Srinivasan, S. Tepavcevic, The phantom menace of dynamic soft-shorts in solid-state battery research, Joule 8 (2024) 64–90.

[243] X. Yang, X. Gao, M. Jiang, J. Luo, J. Yan, J. Fu, H. Duan, S. Zhao, Y. Tang, R. Yang, R. Li, J. Wang, H. Huang, C. Veer Singh, X. Sun, Grain boundary electronic insulation for high-performance all-solid-state lithium batteries, Angew. Chem. Int. Ed. 62 (2023) e202215680.

[244] J. Qu, J. Liu, G. Leng, Y. Wang, S. Wang, S. Shen, H. Yin, Z. Hou, B. Duan, Overcoming the obstacles of lithium-metal anodes for high-energy batteries, Electrochem. Commun. 153 (2023) 107537.

[245] C.D. Fincher, C.E. Athanasiou, C. Gilgenbach, M. Wang, B.W. Sheldon, W. C. Carter, Y.-M. Chiang, Controlling dendrite propagation in solid-state batteries with engineered stress, Joule 6 (2022) 2794–2809.

[246] C.D. Fincher, D. Ojeda, Y. Zhang, G.M. Pharr, M. Pharr, Mechanical properties of metallic lithium: from nano to bulk scales, Acta Mater. 186 (2020) 215–222.

[247] L. Frenck, G.K. Sethi, J.A. Maslyn, N.P. Balsara, Factors that control the formation of dendrites and other morphologies on lithium metal anodes, Front. Energy Res. 7 (2019) 115.

[248] E. Kazyak, R. Garcia-Mendez, W.S. LePage, A. Sharafi, A.L. Davis, A.J. Sanchez, K.-H. Chen, C. Haslam, J. Sakamoto, N.P. Dasgupta, Li penetration in ceramic solid electrolytes: operando microscopy analysis of morphology, propagation, and reversibility, Matter 2 (2020) 1025–1048.

[249] M. Golozar, A. Paolella, H. Demers, S. Savoie, G. Girard, N. Delaporte, R. Gauvin, A. Guerfi, H. Lorrmann, K. Zaghib, Direct observation of lithium metal dendrites with ceramic solid electrolyte, Sci. Rep. 10 (2020) 18410.

[250] K.J. Harry, D.T. Hallinan, D.Y. Parkinson, A.A. MacDowell, N.P. Balsara, Detection of subsurface structures underneath dendrites formed on cycled lithium metal electrodes, Nat. Mater. 13 (2014) 69–73.
[251] C. Yildirim, F. Flatscher, S. Ganschow, A. Lassnig, C. Gammer, J. Todt, J. Keckes, D. Rettenwander, Understanding the origin of lithium dendrite branching in $Li_{6.5}La_3Zr_{1.5}Ta_{0.5}O_{12}$ solid-state electrolyte via microscopy measurements, Nat. Commun. 15 (2024) 8207.
[252] J.-N. Chazalviel, Electrochemical aspects of the generation of ramified metallic electrodeposits, Phys. Rev. A 42 (1990) 7355–7367.
[253] C. Brissot, M. Rosso, J.-N. Chazalviel, S. Lascaud, Dendritic growth mechanisms in lithium/polymer cells, J. Power Sources 81–82 (1999) 925–929.
[254] C. Song, Z. Li, J. Peng, X. Wu, H. Peng, S. Zhou, Y. Qiao, H. Sun, L. Huang, S.-G. Sun, Enhancing Li ion transfer efficacy in PEO-based solid polymer electrolytes to promote cycling stability of Li-metal batteries, J. Mater. Chem. A 10 (2022) 16087–16094.
[255] G. Li, C.W. Monroe, Dendrite nucleation in lithium-conductive ceramics, Phys. Chem. Chem. Phys. 21 (2019) 20354–20359.
[256] H.-K. Kim, P. Barai, K. Chavan, V. Srinivasan, Transport and mechanical behavior in PEO-LLZO composite electrolytes, J. Solid State Electrochem. 26 (2022) 2059–2075.
[257] Y. Huang, D. Perlmutter, A. Fei-Huei Su, J. Quenum, P. Shevchenko, D. Y. Parkinson, I.V. Zenyuk, D. Ushizima, Detecting lithium plating dynamics in a solid-state battery with operando X-ray computed tomography using machine learning, Npj Comput. Mater. 9 (2023) 93.
[258] L. Fan, S. Wei, S. Li, Q. Li, Y. Lu, Recent progress of the solid-state electrolytes for high-energy metal-based batteries, Adv. Energy Mater. 8 (2018) 1702657.
[259] T.H. Dolla, S.O. Ajayi, L.L. Sikeyi, M.K. Mathe, N. Palaniyandy, Advances in solid-state batteries fabrication strategies for their manufacture, J. Energy Storage 106 (2025) 114737.
[260] Q. Li, H. Liu, Y. Ye, K.J. Li, F. Wu, L. Li, R. Chen, The critical importance of stack pressure in batteries, Nat. Energy 10 (2025) 1064–1073.
[261] J. Janek, W.G. Zeier, Challenges in speeding up solid-state battery development, Nat. Energy 8 (2023) 230–240.
[262] Q. Tu, T. Shi, S. Chakravarthy, G. Ceder, Understanding metal propagation in solid electrolytes due to mixed ionic-electronic conduction, Matter 4 (2021) 3248–3268.
[263] Z. Wang, J. Zhao, X. Zhang, Z. Rong, Y. Tang, X. Liu, L. Zhu, L. Zhang, J. Huang, Tailoring lithium concentration in alloy anodes for long cycling and high areal capacity in sulfide-based all solid-state batteries, eScience 3 (2023) 100087.
[264] J.A. Lewis, K.A. Cavallaro, Y. Liu, M.T. McDowell, The promise of alloy anodes for solid-state batteries, Joule 6 (2022) 1418–1430.
[265] S.G. Yoon, B.S. Vishnugopi, D.L. Nelson, A.X.B. Yong, Y. Wang, S.E. Sandoval, T. A. Thomas, K.A. Cavallaro, P. Shevchenko, E.P. Alsaç, C. Wang, A. Singla, J. R. Greer, E. Ertekin, P.P. Mukherjee, M.T. McDowell, Interface morphogenesis with a deformable secondary phase in solid-state lithium batteries, Science 388 (2025) 1062–1068.
[266] S. Moradi, B. Zahiri, P.V. Braun, Cathode chemomechanics controls Li metal solid-state battery performance under low stack pressures, Nat. Commun. 16 (2025) 9266.
[267] C.-L. Tsai, V. Roddatis, C.V. Chandran, Q. Ma, S. Uhlenbruck, M. Bram, P. Heitjans, O. Guillon, Li7La3Zr2O12 interface modification for Li dendrite prevention, ACS Appl. Mater. Interfaces 8 (2016) 10617–10626.
[268] Z. Wang, J. Xia, X. Ji, Y. Liu, J. Zhang, X. He, W. Zhang, H. Wan, C. Wang, Lithium anode interlayer design for all-solid-state lithium-metal batteries, Nat. Energy 9 (2024) 251–262.
[269] Z. Huang, H. Lyu, L.C. Greenburg, Y. Cui, Z. Bao, Stabilizing lithium-metal electrodes with polymer coatings, Nat. Energy 10 (2025) 811–823.
[270] J. Lopez, Y. Sun, D.G. Mackanic, M. Lee, A.M. Foudeh, M.-S. Song, Y. Cui, Z. Bao, A dual-crosslinking design for resilient lithium-ion conductors, Adv. Mater. 30 (2018) 1804142.
[271] C. Wang, H. Wu, Z. Chen, M.T. McDowell, Y. Cui, Z. Bao, Self-healing chemistry enables the stable operation of silicon microparticle anodes for high-energy lithium-ion batteries, Nat. Chem. 5 (2013) 1042–1048.
[272] D.G. Mackanic, X. Yan, Q. Zhang, N. Matsuhisa, Z. Yu, Y. Jiang, T. Manika, J. Lopez, H. Yan, K. Liu, X. Chen, Y. Cui, Z. Bao, Decoupling of mechanical properties and ionic conductivity in supramolecular lithium ion conductors, Nat. Commun. 10 (2019) 5384.
[273] J. Lopez, D.G. Mackanic, Y. Cui, Z. Bao, Designing polymers for advanced battery chemistries, Nat. Rev. Mater. 4 (2019) 312–330.
[274] Y. Sun, J. Lopez, H.-W. Lee, N. Liu, G. Zheng, C.-L. Wu, J. Sun, W. Liu, J. W. Chung, Z. Bao, Y. Cui, A stretchable graphitic carbon/Si anode enabled by conformal coating of a self-healing elastic polymer, Adv. Mater. 28 (2016) 2455–2461.
[275] G. Zheng, C. Wang, A. Pei, J. Lopez, F. Shi, Z. Chen, A.D. Sendek, H.-W. Lee, Z. Lu, H. Schneider, M.M. Safont-Sempere, S. Chu, Z. Bao, Y. Cui, High-performance lithium metal negative electrode with a soft and flowable polymer coating, ACS Energy Lett. 1 (2016) 1247–1255.